ORIGINAL RESEARCH

Linalool-Loaded Glutathione-Modified Gold Nanoparticles Conjugated with CALNN Peptide as Apoptosis Inducer and NF-κB Translocation Inhibitor in SKOV-3 Cell Line

Majid Jabir[1]
Usama I Sahib[1]
Zainab Taqi[1]
Ali Taha[1]
Ghassan Sulaiman [ID][1]
Salim Albukhaty [ID][2]
Ahmed Al-Shammari [ID][3]
Mona Alwahibi[4]
Dina Soliman[4]
Yaser Hassan Dewir[5,6]
Humaira Rizwana[4]

[1]University of Technology, Department of Applied Science, Baghdad, Iraq; [2]University of Misan, Department of Basic Science, Misan, Iraq; [3]Al-Mustansiriyah University, Iraqi Center for Cancer and Medical Genetic Research, Experimental Therapy Department, Baghdad, Iraq; [4]King Saud University, Department of Botany and Microbiology, Riyadh 11495, Saudi Arabia; [5]King Saud University, College of Food and Agriculture Sciences, Riyadh 11451, Saudi Arabia; [6]Kafrelsheikh University, Faculty of Agriculture, Kafr El-Sheikh 33516, Egypt

Background: Linalool is a monoterpene compound with various potential therapeutic applications in several medical fields. Previous studies have indicated the activity of linalool against cell lines; however, its high level of toxicity restricts its use. The aim of this study was to design and manufacture compounds with a novel structure that can be used for loading linalool, to reduce its toxicity and improve its reachable ability.

Methods: We synthesized and characterized a new molecule for loading linalool onto gold nanoparticles (GNPs) capped with glutathione and conjugated with a CALNN peptide. Linalool was loaded onto the GNPs via the reaction of the surface groups of both linalool and the GNPs. Moreover, the target peptide could be loaded onto the surface of the GNPs via a chemical reaction. The cytotoxic effects of linalool–GNP (LG) and linalool–GNP–CALNN peptide (LGC) conjugates against ovarian cancer cells were investigated, as were the possible mechanisms underlying the induction of apoptosis.

Results: Our findings illustrated the significant antiproliferative effect of LG and LGC on SKOV-3 cells. The cytotoxicity assay demonstrated that LG and LGC were selectively toxic in cancer cells and induced apoptosis by activating caspase-8, the p53 protein, and various proteins involved in apoptosis. The present data demonstrated that LG and LGC have a high therapeutic potential and should be given particular consideration as anticancer drug-delivery systems, as LG and LGC were remarkably more cytotoxic against a cancer cell line than were linalool and GNPs alone.

Conclusion: We concluded that LG and LGC are promising compounds that can be used for treating ovarian cancer (SKOV-3) cells via the induction of apoptosis through extrinsic and intrinsic pathways.

Keywords: linalool, gold nanoparticles, CALNN, SKOV-3, p53, caspase-8, NF-κB translocation

Introduction

Drug-delivery systems are a common tool in several therapeutic applications because of advantages such as the bioavailability of the drug, the reduction of the toxicity of the doses required for achieving the optimum response, and the capability of transporting the therapeutic compound into the cell of a particular organ.[1] In the past few years, the majority of research in this field has focused on novel approaches for delivering drugs, depending on the drug-delivery system.[2,3] Cancer

Correspondence: Majid Jabir; Ghassan Sulaiman
Email 100131@uotechnology.edu.iq; 100135@uotechnology.edu.iq

is defined as a disorder in which extraordinary cells are amplified by escaping the traditional regulations of cellular division. Ovarian cancer SKOV-3 cells are a primary type of cancer cells.[4] The exact cause of cancer remains unidentified.[5] Linalool ($C_{10}H_{18}O$) is a monoterpene that can be found in herbs, leaves, flowers, and wood. Linalool essential oil is prepared through chemical synthesis.[6] Several studies have suggested the anticancer activity of linalool against a wide range of cell lines;[7,8] however, its use is restricted by the high toxicity of the essential oil.[9] Recently, glutathione (GSH) has emerged as s popular biodegradable polymer that is used in the preparation of GSH-coated nanoparticles. GSH-coated gold nanoparticles (GNPs) have shown enormous potential as a drug-delivery vehicle. GSH is the most accepted among the different obtainable biodegradable polymers because of its long-standing clinical application, its favorable degradation characteristics, and its potential for sustained drug delivery.[10] Moreover, peptides have been used as targets that can bind with a molecule on the surface of the nucleus and penetrate it. The CALNN pentapeptide consists of the amino acids Cys–Ala–Leu–Asn–Asn.[11] The application of therapeutic peptides depends on several features, including the peptide size and their competence for translocation into the nucleus, as well as high activity, specificity, and affinity.[12] One of the benefits of using peptides in this context is that they do not accumulate in the target organ, which can help reduce the toxic side effects of the drug.[13] In a study reported by Jabir (2018),[14] a novel method for manufacturing GNPs and loading linalool onto them was investigated, and the results confirmed the high effectiveness of the manufactured compound in affecting the bacterial cell membrane, thus leading to the loss of cell integrity and the increase in the permeability of the cell wall, in addition to enhancing the formation of reactive oxygen species (ROS), which play a major role in damaging bacterial DNA. The efficiency of linalool-loaded GSH-modified GNPs conjugated with a CALNN peptide against breast cancer cells (MCF-7) was also investigated by Jabir (2019);[15] in that study, the authors presented an effective compound that had a great potential to be considered as an anticancer delivery system against a breast cancer cell line, as LIN-GNP-CALNN could make their way into the nucleus, whereas CALNN was mostly trapped in the endoplasmic reticulum because of the higher affinity of the ER signal to peptides and its ability to penetrate the nucleus.[15] Cancer is a lethal disease with no geographical or organ limitations that results in a worldwide annual mortality exceeding 12.7 million people. Among women, breast and ovarian cancers are responsible for at least 15–17% of the entire cancer cases and approximately 23% of the invasive types, thus representing the most widely prevailing invasive cancers among women. Apoptosis is a critical and important cellular homeostatic process that modulates the mechanism involved in the regulation of the population size of various cell types, and the upregulation of several apoptotic markers may elicit DNA damage and inhibit the progression of tumor cells.[16] This study was conducted to develop a new drug-delivery system that consisted in loading linalool onto GNPs capped with GSH and then conjugated with a CALNN peptide, to reduce its toxicity. We then investigated the activity of these GNPs against the SKOV-3 cell line as a novel therapeutic approach to explain the possible mechanism underlying the killing of ovarian cancer cells, which included apoptosis through the upregulation of p53 and the downregulation of NF-κB. Finally, we investigated the apoptosis pathway using a proteome profiler array to determine the involvement of proteins related to apoptosis in this process.

Materials and Methods
Synthesis of GSH-Capped Gold Nanoparticles
Tetrachloric acid (8.5 mg.mL^{-1}) (Riedel-DeHaen AG, Germany) was mixed with GSH (Riedel-DeHaen AG, Germany) (5.84 mg.mL^{-1}). The pH value of the combination was set to 8. Sodium borohydride (2 mg) was used as a reducing agent. The reaction was allowed to continue overnight, after which the mixture was centrifuged at 10,000 rpm to remove the excess reactants.[17]

Synthesis of Linalool–GSH-Capped Gold Nanoparticles
Linalool (1.54 mg.mL^{-1}) (Sigma, USA) was combined with the prepared nanoparticles. The pH of the mixture was adjusted to 5. The mixture was stirred for 12 h at 25°C, followed by centrifugation at 13,000 rpm for 15 min in a cooled centrifuge (4°C), to remove excess linalool from the complex.[14]

Synthesis of the Linalool–Gold Nanoparticle–CALNN Conjugate
The prepared LG was combined with CALNN (1.38 mM) (University of Ioannina, Greece) at a ratio of 10:1. This

combination was stirred overnight at room temperature and then centrifuged at 13,000 rpm for 30 min, to remove the excess reactants.[18]

Characterization of the Synthesized Compounds

The synthesized compounds were analyzed using a UV-sp -8001 spectrophotometer at a scanning wavelength of 200–1000 nm. The morphological characteristics were identified by scanning electron microscopy (SEM) and transmission electron microscopy (TEM).

Drug-Release Profile

The release profile of the synthesized compounds was assessed. In brief, 5 mg of LG and LGC were dissolved in 5 mL of phosphate-buffered saline at 37°C for different periods. After preparing the samples, the absorbance of linalool was measured using a spectrophotometer at a wavelength of 320 nm over time.[19]

In vitro Evaluation of Antioxidant Potential

DPPH Scavenging Assay

The scavenging capacity of the synthesized compounds was evaluated using a stable DPPH procedure (Sigma–Aldrich, USA).[20] A total of 500 μL of the synthesized compounds was added to 500 μL of DPPH, and the volume was made up to 2 mL using absolute ethanol. The absorbance of each compound was measured at 517 nm.

Resazurin Dye Scavenging Assay

The ability of the synthesized compounds to scavenge free radicals was analyzed using the resazurin dye (Himedia, India).[21] The synthesized compounds (10 μg.mL^{-1}) were mixed with an equal volume of resazurin dye. The absorbance of resazurin was measured 15 min later at a wavelength of 600 nm against a blank solution containing only DW.

Identification of the Cytotoxic Effect of the Synthesized Compounds

Maintenance of SKOV-3 Cells

The human ovarian cancer cell line SKOV-3 was obtained from the Cell Bank of the Iraqi Center for Cancer and Medical Genetic Research, and was maintained in RPMI-1640 medium (Gibco, USA) supplemented with 5% calf bovine serum, penicillin (100 U.mL^{-1}), streptomycin (100 μg.mL^{-1}), and trypsin–EDTA (Biosource, Belgium). These components were used for the passaging of cells and reseeding twice a week (50% confluence), and cells were incubated at 37°C.

Cell Proliferation Assay

The proliferation of the ovarian cancer cells (SKOV-3) was investigated after treatment with 10 μg.mL^{-1} of linalool, GNPs, linalool-loaded GNPs (LG), and linalool-loaded GNPs conjugated with a CALNN peptide (LGC). Cells were labeled with a cell proliferation kit for flow cytometry (CellTrace™ Red-APC) before exposure to the compounds, according to the kit protocol (ThermoFisher Scientific). After centrifugation, SKOV-3 cancer cells (10^6) were resuspended in PBS (1 mL) (OXOID, England) with the addition of CellTrace™ (0.25 μL), followed by incubation for 20 min in the dark. Culture medium (5 mL) was added to the prepared samples and cells were incubated for 5 min. After incubation, the cells were washed, seeded into a 96-well plate containing the synthesized compounds at a concentration of 10 μg.mL^{-1}, and incubated for 96 h. After the incubation, the cells were detached and analyzed by flow cytometry.

MTT Assay

The cytotoxic effect of the synthesized compounds at different concentrations of 10 μgmL^{-1} was determined.[22] Briefly, 5×10^4 cells were seeded into 96-well plates and incubated overnight at 37°C, to facilitate cell adherence to the plate's surface. Subsequently, 10 μgmL^{-1} of each of the compounds was transferred to the wells and cells were cultured for 48 h. MTT solution (Sigma–Aldrich, USA) was added to the cells. After the incubation period, the medium was aspirated, and DMSO (Sigma–Aldrich, USA) solution was added to each well. The absorbance of each well was measured at a wavelength of 492 nm using a microplate reader.

Clonogenicity Assay of SKOV-3 Cells

SKOV-3 cells were seeded into 24-well plates at a density of 800 cells mL^{-1}. Twenty-four hours later, the cells were treated with 10 μg.mL^{-1} each of linalool, GNPs, LG, and LGC. The medium was discarded when the cells reached monolayer confluence, followed by rinsing using PBS. The colonies were fixed with methanol (96%), stained with crystal violet (Sigma–Aldrich, USA), and washed with tap water to remove excess dye, and then photographed.[23]

Identification of Changes in Nuclear Morphology

Changes in nuclear morphology in the treated cell line were investigated using fluorescent staining (DAPI, Sigma–Aldrich, USA). Cells were cultured in 96-well plates and allowed to adhere for 24 h in a 5% CO_2 incubator. Subsequently, the cells were treated with the compounds at a concentration of 10 µg.mL^{-1}, followed by incubation for 48 h. After the incubation, the cells were rinsed with PBS and fixed with absolute ethanol. After a 30-min incubation in ethanol, the cells were rinsed again with PBS, followed by DAPI staining and incubation for 30 min.[19] The changes in the morphological characteristics of the nucleus were observed under a fluorescence microscope.

Acridine Orange–Ethidium Bromide Staining

The compound-induced death of SKOV-3 cells was assessed using the AO/EtBr (Sigma–Aldrich, USA) staining method.[15] Briefly, 24 h after the seeding of cells in 12-well plates, they were treated with 10 µg.mL^{-1} LG and LGC and incubated for an additional 20 h. The cells were washed twice with phosphate-buffered saline. Dual fluorescent dyes (10 µL) were added into the wells at an equal volume of cells. Finally, the cells were observed using fluorescence microscopy.

Apoptosis Assay

SKOV-3 cells (1×10^5/mL) that were treated with each of the synthesized compounds at a concentration of 10 µg. mL^{-1} were removed and transferred to sterilized tubes, followed by washing twice with Annexin V buffer solution by centrifugation (1000 rpm).[24] For cell-cycle analysis, cells were fixed in 70% ethanol/PBS and centrifuged. For apoptosis detection, cells were dispersed in 1× Annexin V binding buffer with Annexin V-FITC/PI stain (Sigma–Aldrich, USA) for 15 min in the dark, and then subjected to flow cytometry. Dead ovarian cancer cells that were labeled with Annexin V-FITC/PI were identified as having undergone apoptosis. Flow cytometry was used to analyze these phenomena with the FACSDiva^{TM} software. Finally, the outcome data were analyzed using the FlowJo software.

Identification of DNA Damage
Genotoxicity Assay

The genotoxicity effect of the synthesized compounds on DNA was investigated using the alkaline comet assay.[25] Briefly, SKOV-3 cells treated with 10 µg.mL^{-1} of the synthesized compounds were harvested and concentrated in LMAgarose (Trevigen, USA) in the molten state at a concentration of 1×10^5 mL^{-1} and a ratio of 1:10 (v/v) at 37°C. Subsequently, the prepared samples were transferred to the comet's slide. These slides were immersed in a lysis solution (4°C, 1 h), followed by the addition of an alkaline unwinding solution (pH >13.0, room temperature, 20 min). After completing the preparation steps, the slides were placed on an electrophoresis slide tray containing NaOH-EDTA solution. Electrophoresis was performed under suitable conditions (21 V, 30 min). The cells present in the circle of dried agarose were stained with SYBR Green solution (room temperature, 30 min). After the completion of the staining steps, a confocal laser scanning microscope was used to visualize the samples. The outcome data were analyzed using the Comet Assay Software.

DNA Fragmentation Assay

The DNA fragmentation assay was performed according to the manufacturer's protocol. SKOV-3 cells at a density 1×10^6 cells.mL^{-1} were treated with the synthesized compounds for 24 h. The cells were detached and suspended in phosphate-buffered saline. Centrifugation (1200 rpm, 4°C, 10 min) was performed to remove the medium, followed by dissolution in DNA-loading buffer and application onto an 0.8% agarose gel. Electrophoresis was performed, followed by staining with ethidium bromide. Nucleic acid fragmentation was observed using a UV illuminator device.

Production of ROS

ROS production in SKOV-3 cells treated with linalool, GNPs, LG, and LGC was determined using a cellular ROS detection assay kit (Abcam, Cambridge, UK; ab113851). Briefly, SKOV-3 cells were seeded into 48-well plates at a density of 5×10^5 per well. Then, the cells were treated with the test compounds and incubated for 24 h at 37°C. The cells were washed twice with PBS, stained with dihydroethidium (DHE) dye for 1 h, and washed with washing buffer. The formation of ROS was examined under a fluorescence microscope.

Identification of the Localization of the Synthesized Compounds in SKOV-3 Cells

Nanoparticles labeled with a fluorescent stain were prepared using the following technique. In brief, FITC (Sigma–Aldrich, USA) at a concentration of 1 mg.mL^{-1} was mixed with LG or LGC and then incubated at room

temperature for 10 h. The reaction was quenched using Tris buffer (pH 10). FITC-labeled cells were collected by centrifugation and washed three times with DMSO to remove unbound FITC. FITC-labeled LG and LGC were added to cells, which were then incubated at 37°C for 12 h. DAPI staining was used to stain the nuclei. Images were acquired at a magnification of 40×using a fluorescence microscope.[15] SEM was used to confirm the internalization of LG and LGC into SKOV-3 cells. In brief, SKOV-3 cells were treated with LG and LGC for 24 h and then washed with PBS. Cells were immersed in a 2.5 vol% glutaraldehyde/PBS solution and kept at 4°C for 8 h, for fixation. The samples were then washed twice with PBS, dehydrated using different concentrations of ethanol, treated with 100% hexamethyldisilazane for 10 min, and finally left to dry. The morphology of SKOV-3 cells was examined using SEM.

Mitochondrial Membrane Potential Assay
Qualitative and quantitative changes in MMP were evaluated by JC-1 staining (Sigma–Aldrich, USA). Cells were treated with each of the compounds at a concentration of 10 µg.mL^{-1}. After treatment, cells were incubated with 5 mM JC-1 stain for 30 min at 37°C and then washed, and images were acquired using a fluorescence microscope. The intensity of the fluorescence in each treatment condition was estimated using the NIH ImageJ software. To confirm the effect of the tested compounds on the mitochondrial function of SKOV-3 cells, the rhodamine (Rh123) fluorescent dye was used. This dye was used to examine the membrane potential of the mitochondria before and after treatment with the test compounds. In brief, 24 h after the seeding of cells in 96-well plates, they were treated with the active compound and stained with 5 M Rh123 dye for 2 h at 37°C. Subsequently, the cells were detached using 0.2 mL of 5% trypsin–EDTA and then centrifuged at 300 rpm for 5 min. Cells were then resuspended in FACS buffer and evaluated by flow cytometry assay, and histograms were plotted.

Proteomic Profiler Array for Identifying Apoptosis
To investigate the possible pathway of apoptosis triggered by LGC, a proteomic profiler array (RayBio, human apoptosis Antibody Array C1 Kit) was used for determining the involvement of proteins related to apoptosis. SKOV-3 cells were treated with the synthesized compounds (10 µg. mL^{-1}, 24 h). The proteins (250 µg) extracted from treated and nontreated cells were incubated overnight with the human apoptosis antibody array. The membranes used for quantifying the apoptosis array data were scanned on a Biospectrum AC ChemiHR apparatus. The results obtained from the membranes were analyzed using the ImageJ software, and the signal-fold expression levels of each sample were estimated according to the manufacturer's instructions.

Measurement of Caspase-8 and p53 Levels
Flow Cytometry Assay
The activation states of caspase-8 and p53 were evaluated using a fluorescein caspase-8 and p53 staining kit (Thermo Fisher Scientific, USA). Briefly, SKOV-3 cancer cells (4×10^4 cells.mL^{-1}) were cultured in 5 mL of medium and incubated for 24 h at 37°C. Next, the incubated cells were exposed to each of the compounds (10 µg.mL^{-1}) for 24 h. After the incubation period, the treated cells were harvested and washed twice with 1× ice-cold PBS. The pellets were collected and the cell density was reset (1×10^6 cells.mL^{-1}) using growth medium. The prepared cells were then incubated with 1 mL of FITC-IETD-FMK at 37°C for 60 min, which was used for the identification of caspase-8 and FITC-anti-p53. After the incubation period, the cells were washed twice with wash buffer (0.5 mL). The stained cells were transferred to flow cytometry tubes and subjected to flow cytometry. Data were calculated and analyzed using the BD Accuri C6 software.

Real-Time PCR
The treated SKOV-3 cells were also evaluated regarding the expression levels of the p53 and caspase-8 mRNAs using QPCR. The primer sets used in our study were determined based completely on the standard sequences obtained from the NCBI database. The sequences of primers used in the quantitative RT–PCR assay were as follows: 1, P53 (forward: 5′–CCGTCCCAAGCAATGGATG–3′; reverse: 5′–GAAGATGACAGGGGCCAGGAG–3′); 2, Caspase-8 (forward: 5′–GACCACGACCTTTGAAGAGCTTC–3′; reverse: 5′–CAGCCTCATCCGGGATATATC–3′). Total RNA was purified from the cells according to the supplier's protocol (RNeasy Mini kit, Qiagen. Cat. No. 74,104, UK) and treated with DNase, and the product was treated with Superscript II reverse transcriptase for the synthesis of cDNA (Invitrogen. Cat. No. 18,064–071, USA). For quantitative reverse transcription polymerase chain reaction (qRT–PCR), each reaction mixture contained 1 µL of cDNA, 7.5 µL of SYBR green, 0.3 µL of ROX, and 0.3 µL of related primers; the final volume was made up to 15

μL by adding 5.6 μL of distilled water. The fast SYBR Green master mix was used (Applied Biosystems. Cat. No. 4,385,612, UK) together with the 7900HT fast system (Applied Biosystems). After the normalization of the expression levels of genes to that of the gene encoding the TATA-binding protein, their mean relative values were calculated based on reported methods (Livak and Schmittgen).

Measurement of NF-κB Activity

The inhibitory activity of NF-κB through LG and LGC was analyzed using the CellomicsArray Scan HCS system. This assay was performed using the Cellomics NF-κB activation kit (Thermo Fisher Scientific, USA).[20] After treatment of the SKOV-3 cancer cells with LG and LGC (10 μg.mL^{-1}, 24 h), TNF-α (10 ng.mL^{-1}, 30 min) was used for stimulation. After the treatment period, fixation and staining were performed according to the kit protocol. The Array Scan HCS Reader and Cytoplasm to Nucleus Translocation Bioapplication software were used for data analysis.

Statistical Analysis

GraphPad Prism 6 was used for the statistical analysis of the data, which were presented as the mean ± SEM of three replicates per experiment.[26]

Results and Discussion

Synthesis and Characterization of GNPs, LG, and LGC

The synthesis of GNPs was performed according to the chemical reaction assay. GSH reacts with HAuCl$_4$ as a capping agent that can cap the gold salt and form an abundant polymer by changing the pH scale range to 8. The repulsive electrostatic force between GSH causes less aggregation.[27] Finally, GNPs are formed by the addition of NaBH$_4$. NaBH$_4$ acts as a reducing agent that can split the GSH polymer into monomers.[28] Figure 1 shows the dimensions of GNPs, which were estimated using the ImageJ software. The results showed that the particle size was around 5 nm. Moreover, LG and LGC showed a slightly increased diameter, and their dimensions were 11 and 13 nm larger than the particles observed in GNPs, respectively. Tetrachloric acid is a yellow-colored solution that changes to a red color after the addition of NaBH$_4$. Moreover, the synthesis of linalool-loaded GNPs (LG) was performed according to the isoelectric point (pI). The pI value of GSH is 5.93. It is easy to make GSH lose a hydrogen atom by modifying the pH scale range to 5.[14] The linalool-loaded gold complex was visualized as having a turbid color. Linalool-loaded GNP–CALNN (LGC) was synthesized
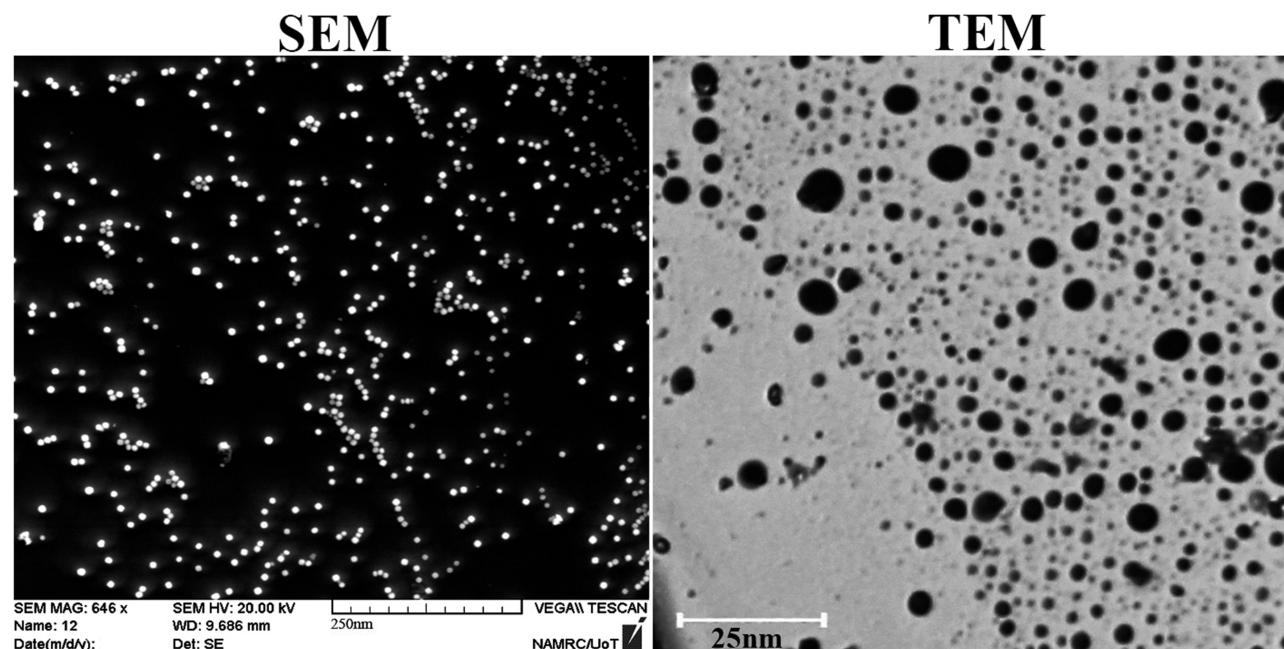

Figure 1 Physical characterisation of gold nanoparticles. Scanning electron microscopy images of gold nanoparticle (scale bar: 250 nm) and transmission electron microscopy (scale bar: 25 nm).
Abbreviations: SEM, scanning electron microscopy; TEM, transmission electron microscopy.

based on the chemical reaction between the C=O bond of linalool-loaded gold and the NH bond of the peptide.[18] The visible color of LG turned colorless (non-color) after the inclusion of the CALNN peptide. UV and visible absorption spectroscopy revealed the change in the absorbance of the synthesized compounds, as shown in Figure 2A. The top peak of GNPs can be observed in the 535 nm region.[29] Linalool is a colorless solution, and the sharp band can be observed at almost 320 nm.[30,31] In turn, LG displays a color change from red to turbid, and the top band can be observed at almost 280 nm. After conjugating the target peptide with LG, the color shifted to colorless, and the top wavelength was in the 300 nm region. Figure 2B depicts the drug-release profile of LG and LGC. Several periods were used to identify the drug-release profile. The outcome data showed that, for LG, a higher percentage of released drug could be achieved after 1440 min, with a cumulative release ratio of 78.7%. Moreover, LGC yielded a higher drug-releasing
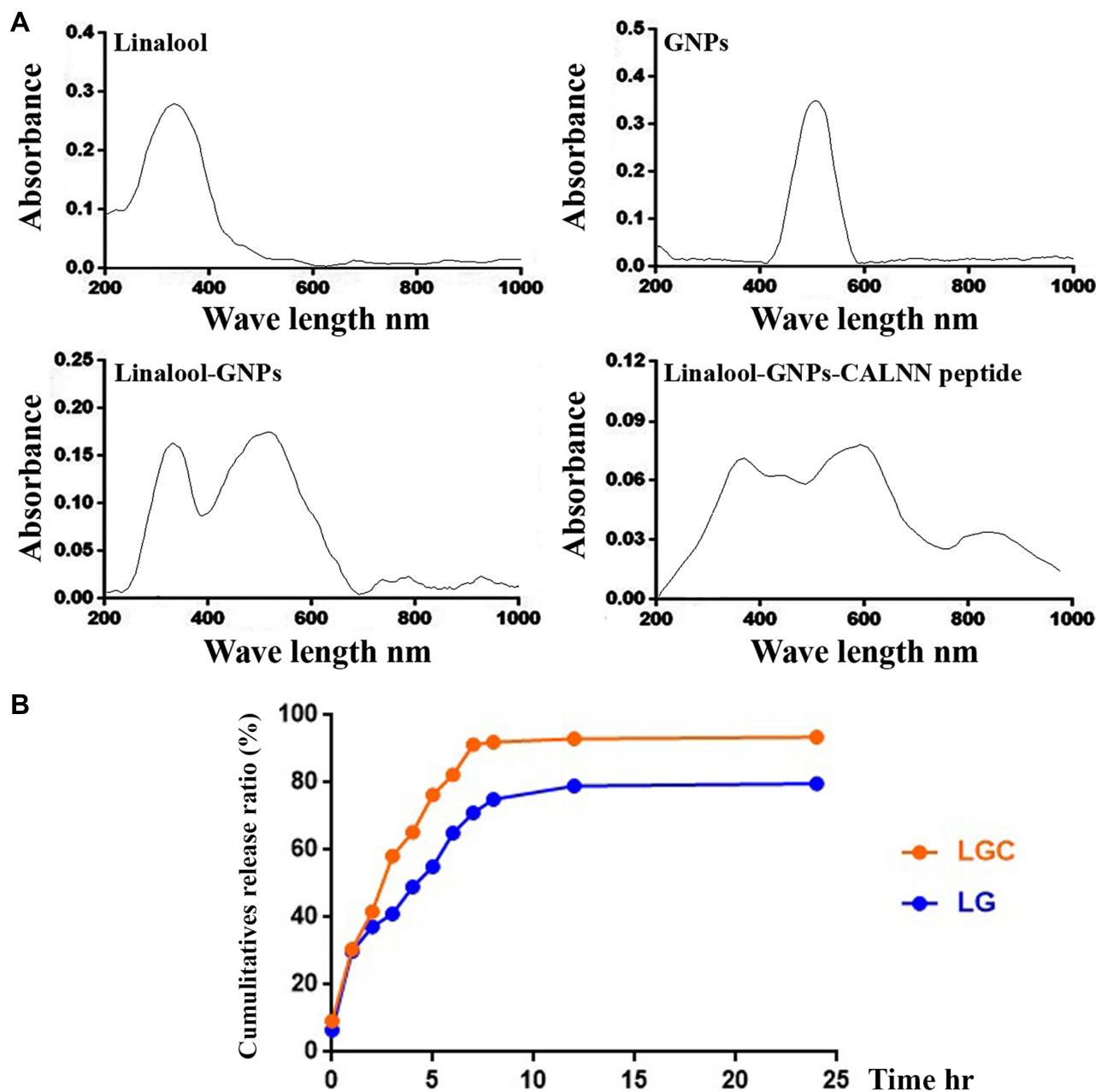

Figure 2 Characterization of of the synthesised compounds. (**A**) UV-VIS spectroscopy analysis of linalool, gold nanoparticles, LG, and LGC. (**B**) Drug release profile of LG and LGC.
Abbreviations: GNP, gold nanoparticle; LG, linalool-gold nanoparticle; LGC, linalool-gold nanoparticle-CALNN.

percentage compared with LG, with the cumulative ratio reaching 93.2% after 1440 min. The sustained release of a drug in a delivery system is an important property that is closely related to pharmacokinetics and therapeutic efficacy.[32]
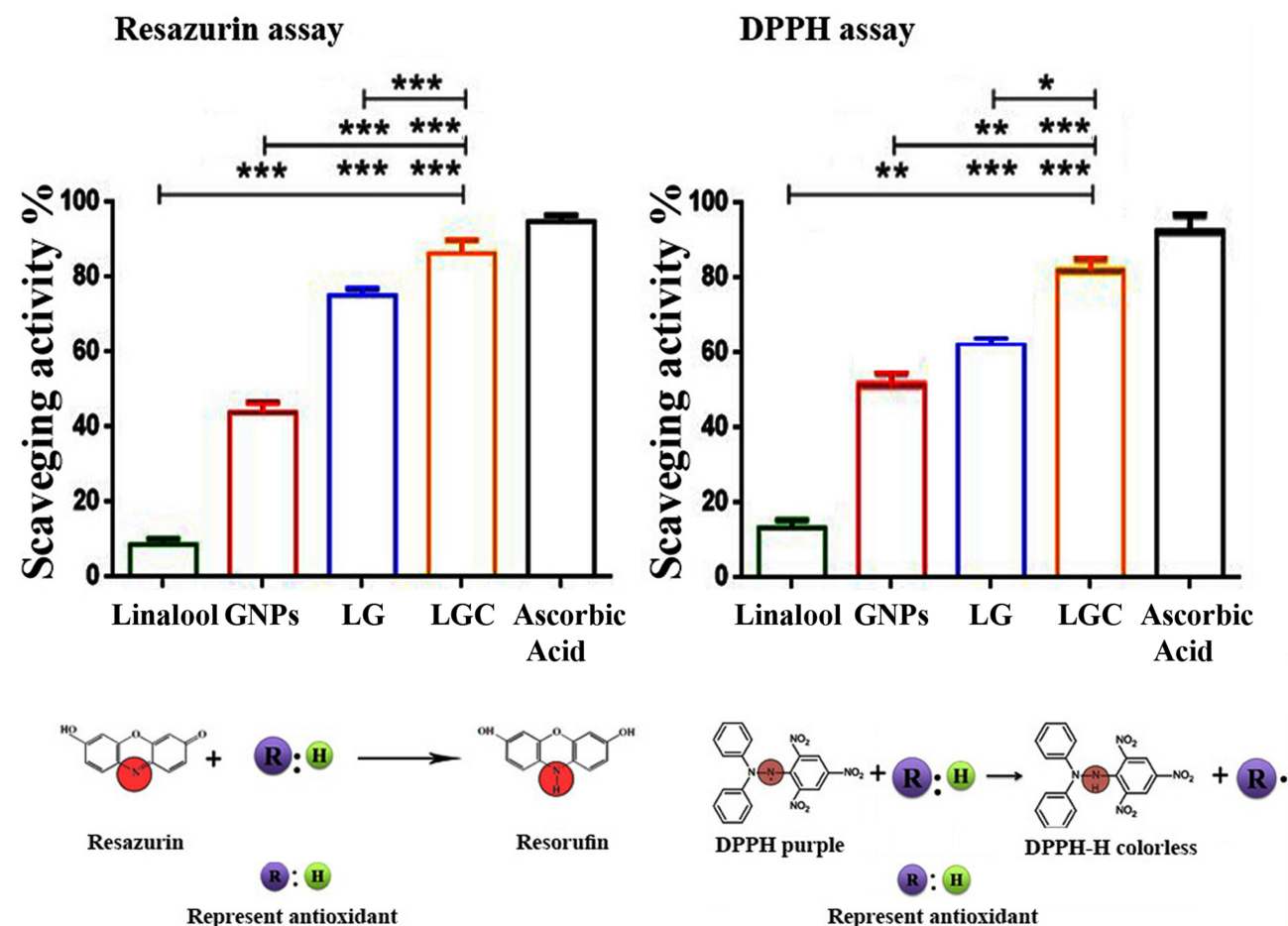
In vitro Evaluation of Antioxidant Potential

The antioxidant activity of each compound was investigated using two experimental assays: DPPH and resazurin staining. DPPH (2,2-diphenyl-1-picrylhydrazyl) has a reliable free radical related to a spare electron.[33,34] The DPPH radical-scavenging (%) activities are shown in Figure 3. Linalool exhibited a weak antioxidant activity (18.3%); the poor activity of the oil may be attributed to the weak ability of its primary components to scavenge DPPH free radicals.[35] The scavenging activity of GNPs reached 48.3%.[36] Based on the excessive surface vicinity, it appears

that nanoparticles have an excessive tendency to interact with free radicals.[37] LG exhibited a high scavenging activity of up to 74.1%, and LGC showed the highest scavenging activity, which reached 81.2% compared with other samples. In the resazurin staining assay, the stain confers a blue color that becomes pink when reduced to resorufin.[38] As observed in Figure 3, linalool had a low scavenging activity (8.02%), whereas that of GNPs and LG was 43.97% and 74.97%, respectively, compared with ascorbic acid (93.4% scavenging activity). Moreover, LGC exhibited a high scavenging activity of 83.3%. The high scavenging activity of LG and LGC may be related to the high surface area and the ability to donate hydrogen electrons to the nitrogen radical.

Cytotoxic Effect of the Synthesized Compounds Against SKOV-3 Cells

The toxicities of linalool, GNPs, linalool-loaded GNPs (LG), and linalool-loaded GNP–CALNN peptide (LGC)

Figure 3 Antioxidant activity of the synthesised compounds. Upper lane represented the antioxidant percentage and Lower lane represented the principle of each assay. The results are represented as the mean ± SD. Asterisks indicate statically different, *p≤0.05, **p≤0.01, ***p≤0.001.
Abbreviations: DPPH, 2, 2 diphenyl 1 picrylhydrazyl; LG, linalool-gold nanoparticle; LGC, linalool-gold nanoparticle-CALNN.

against ovarian cancer cells were determined according to the characterization of the synthesized compounds. The antitumor effects of the synthesized compounds were strengthened by their capability to prohibit tumor cell proliferation. As shown in Figure 4A, LG and LGC had a greater capability to prevent and inhibit the proliferation of ovarian cancer cells than did linalool or GNPs alone. The cytotoxic effects of LG and LGC on the ovarian cancer cell line SKOV-3 after 48 h of exposure are shown in Figure 4B. The results demonstrated that treatment with LG and LGC inhibited cell growth ($P \leq 0.01$ and $P \leq 0.001$, respectively), and that both LG and LGC were more potent than linalool alone. LG and LGC exhibited a cytotoxic activity >72%. Linalool was slightly efficient on the cell line, whereas GNPs exhibited moderate antiproliferative efficiency. This study suggests that GSH, which capped the GNPs and CALNN peptide, enhanced the delivery of linalool into cells and led to increased water solubility and bioavailability, thus causing linalool to exhibit enhanced cell growth inhibition compared with that described in other studies, which reported the cytotoxic effects of linalool and GNPs on various cancer cell lines.[39] In contrast, LIN–GNPs and LIN–GNPs–CALNN targeted different organelles in living cells; LIN–GNPs showed a high activity because of their small size. Moreover, electrically charged nanoparticles may have exhibited better association and internalization rates as a result of the electrostatic interaction between the electrically charged cell membrane and the charged particles.[15] Our results suggest that these compounds can be considered as a particularly valuable source of active antiproliferative and cytotoxic agents. Morphological changes were investigated in SKOV-3 cells using a phase-contrast inverted microscope after staining with crystal violet. The control cells retained their original morphology, whereas the cancer cells stopped proliferating after treatment with the test compounds and exhibited fragmentation of chromatin, bleb formation on the cell surface, cytoplasmic shrinkage, loss of cell-to-cell contact, and a reduction in their density, which are representative apoptotic features.[40,41] Figure 4C presents the antiproliferative effects of the synthesized compounds on SKOV-3 cells, thus further confirming the cytotoxic effect of these compounds. LG and LGC exhibited high activity in suppressing the colony-formation ability of SKOV-3 cells compared with linalool and GNPs, which exhibited only a modest efficiency. The reduction in colony formation indicated that the cells that were subjected to continuous

treatment were killed within 48 h, suggesting that LG and LGC were taken up by cells and led to the induction of apoptotic mechanisms.[42,43] Therefore, our results indicated that the synthesized compounds induced cell death. Nonetheless, the cell death mechanism was not clearly apparent and, thus, warranted further investigation.

Identification of Changes in Nuclear Morphology

To evaluate the cytotoxic effects of the compounds regarding the nuclear morphology, fluorescent staining (DAPI) and AO-ET were used for detecting changes in nuclear morphology; in addition, Annexin V-FITC was used to determine the percentage of apoptotic cells. The changes in nuclear morphology were examined after treating the ovarian cancer cells with the synthesized compounds and staining with DAPI, as shown in Figure 5A. In contrast, apoptosis is characterized by cellular shrinkage, preservation of plasma membrane integrity, condensation of chromatin, and fragmentation of the nucleus.[44] Overall, our results suggest that LG and LGC can induce apoptosis in ovarian cancer cells. The reduction of cell growth often involves the modification of various important signaling pathways, which is caused by the induction of a programmed cell death mechanism that affects gene expression levels.[45] Moreover, the nuclear morphology of treated cells was evaluated using acridine orange–ethidium bromide dual staining. Apoptotic cells were evaluated based on DNA damage. In this study, the efficiency of the synthesized compounds was also investigated. AO-EB staining was used to examine the different apoptotic features of the nuclear alterations. Nonapoptotic cells appeared green in color, and apoptotic cells appeared orange or red in color after staining with AO-EtBr.[46] As shown in Figure 5B, the cells treated with the synthesized compounds showed an increase in cell membrane disruption and number of vacuoles during lysosome formation compared with nontreated cells. The flow cytometry analysis revealed that cells undergoing apoptosis were labeled with Annexin V in quadrant Q3. Figure 5C shows the dot plots of SKOV-3 cells challenged by the compounds for 24 h. In the untreated control sample, the majority (88.7%) of cells were viable and nonapoptotic, whereas among the linalool-treated cells, the nonapoptotic cell percentage was 79.1% and the apoptotic cells reached 17.5%. In turn, 70.4% and 29.4% of the cells treated with GNPs were nonapoptotic and apoptotic cells, respectively. Moreover, among the cells treated with
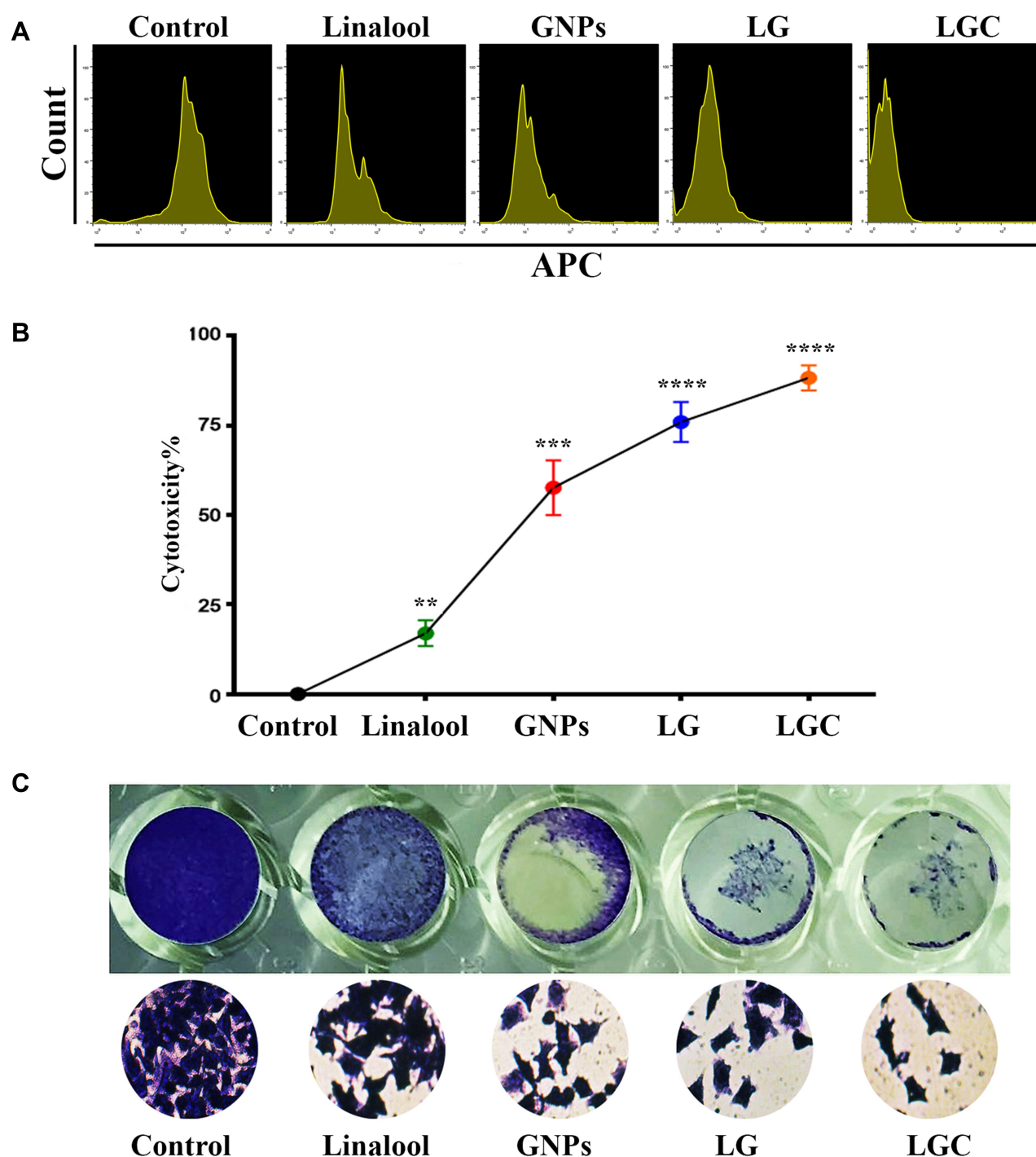
Figure 4 Antiproliferative activity of test compounds against SKOV-3 cell line. (**A**) Representative proliferation assay by CellTrace™, Each peak represents the cell division and consequently dilution of CellTrace into the cytoplasm. (**B**) Cytotoxic effect of tested compound on SKOV-3 human ovarian carcinoma cells after 48 h. (**C**) Colony-forming unit of SKOV-3 cell line treated as indicated for 24 h. The results are represented as the mean ± SD. Asterisks indicate statically different from control, **p≤0.01, ***p≤0.001, ****p≤0.0001.
Abbreviations: GNP, gold nanoparticles; LG, linalool-gold nanoparticle; LGC, linalool-gold nanoparticle-CALNN.

the LG complex, 49.8% were apoptotic and 46.6% were nonapoptotic cells. Finally, among the cells treated with the LGC complex, 57.9% were apoptotic and 38.5% were nonapoptotic cells. There was a decrease in the Annexin V$^-$ PI$^-$ population and an increase in cells undergoing apoptosis,

which showed an increase in the Annexin V$^+$ PI$^+$ population, indicating that dead or necrotic cells were observed after treatment with LG and LGC. The Annexin V$^+$ PI$^+$ and V$^+$ PI$^-$ gate referred to late apoptosis. These results indicated the high capability of LGC to induce cell death
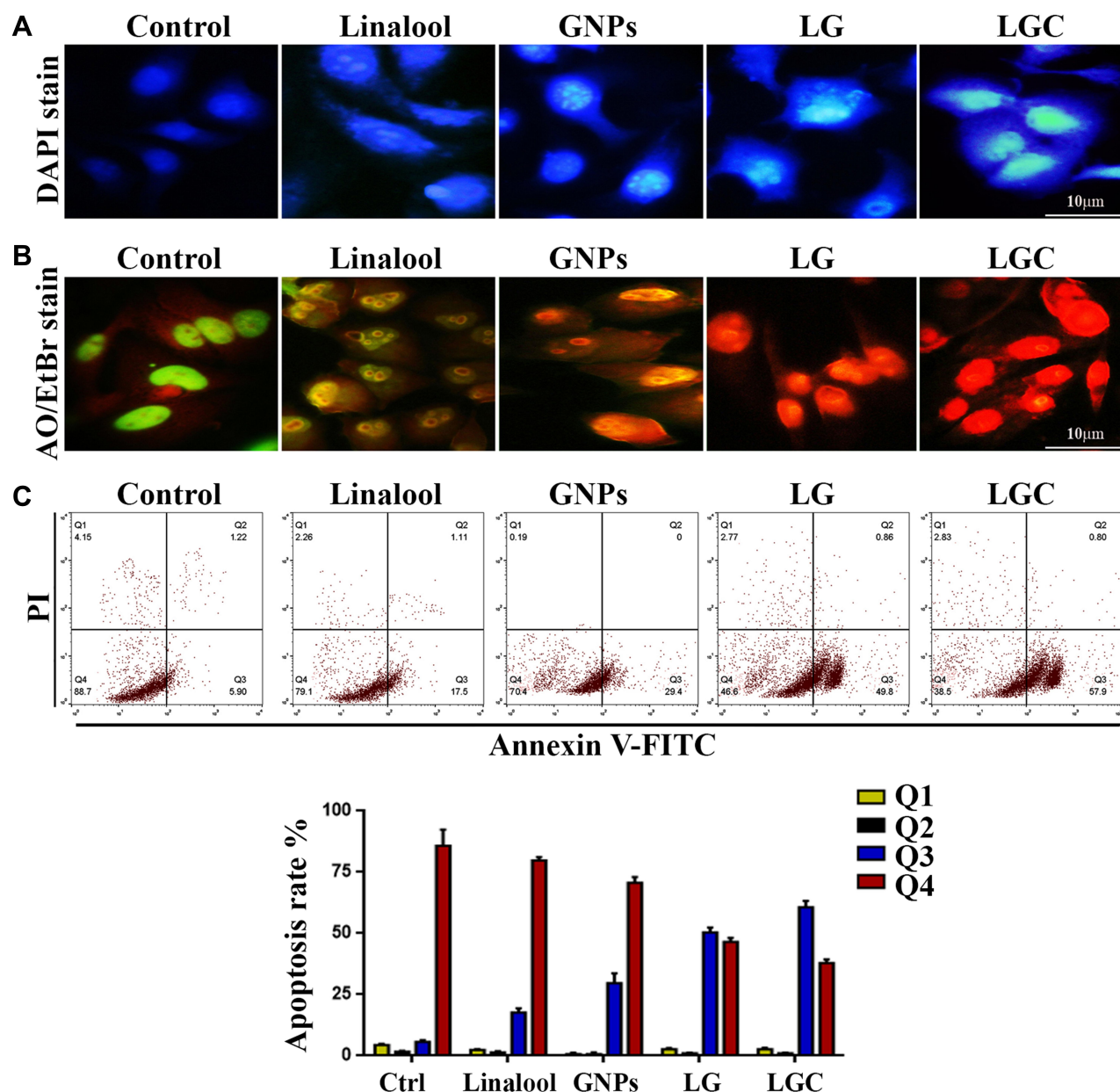
Figure 5 Apoptosis markers in treated SKOV-3 cells following treatment with tested compounds as indicated. (**A**) Microscopic tracking of nuclear morphology by staining of DAPI (nucleus), treated cells with LG and LGC increased the fluorescent intensity of nuclear. (**B**) SKOV-3 cells treated as indicated. Untreated cells are shown normal structure of cell without significant apoptosis or necrosis, after treated, apoptosis features including blebbing and chromatin condensation were observe, and can see red color that detect the apoptosis. (**C**) Flow cytometric analysis of early and late apoptosis. The treated cell were analyzed after staining with FITC-conjugated AV and PI by flow cytometer. Chart bar represented % of apoptosis rate in SKOV-3 cells after treated as indicated. The results are represented as the mean ± SD.
Abbreviations: DAPI, 4′,6-diamidino-2-phenylindole; FITC, fluorescein isothiocyanate; AO-ET, acridine orange ethidium bromide; AV, annexin V; PI, propidium iodide; GNP, gold nanoparticles; LG, linalool-gold nanoparticle; LGC, linalool-gold nanoparticle-CALNN.

because of the competency of nanoparticles to penetrate the nuclear membrane and cause changes in the mRNA expression levels of the following five genes, which are involved in the regulation of the apoptotic pathways: *p53, Bax, bcl-2, caspase-3*, and *caspase-9*. Our results also showed that apoptosis was induced in SKOV-3 cells after exposure to LG and LGC. It is important to emphasize that the apoptotic effects of LG and LGC were stronger than those of the other compounds alone.

Identification of DNA Damage

The DNA damage based on the severity of the destruction and tail length of SKOV-3 cells are shown in Figure 6. In addition to their role in apoptosis, LG and LGC have been
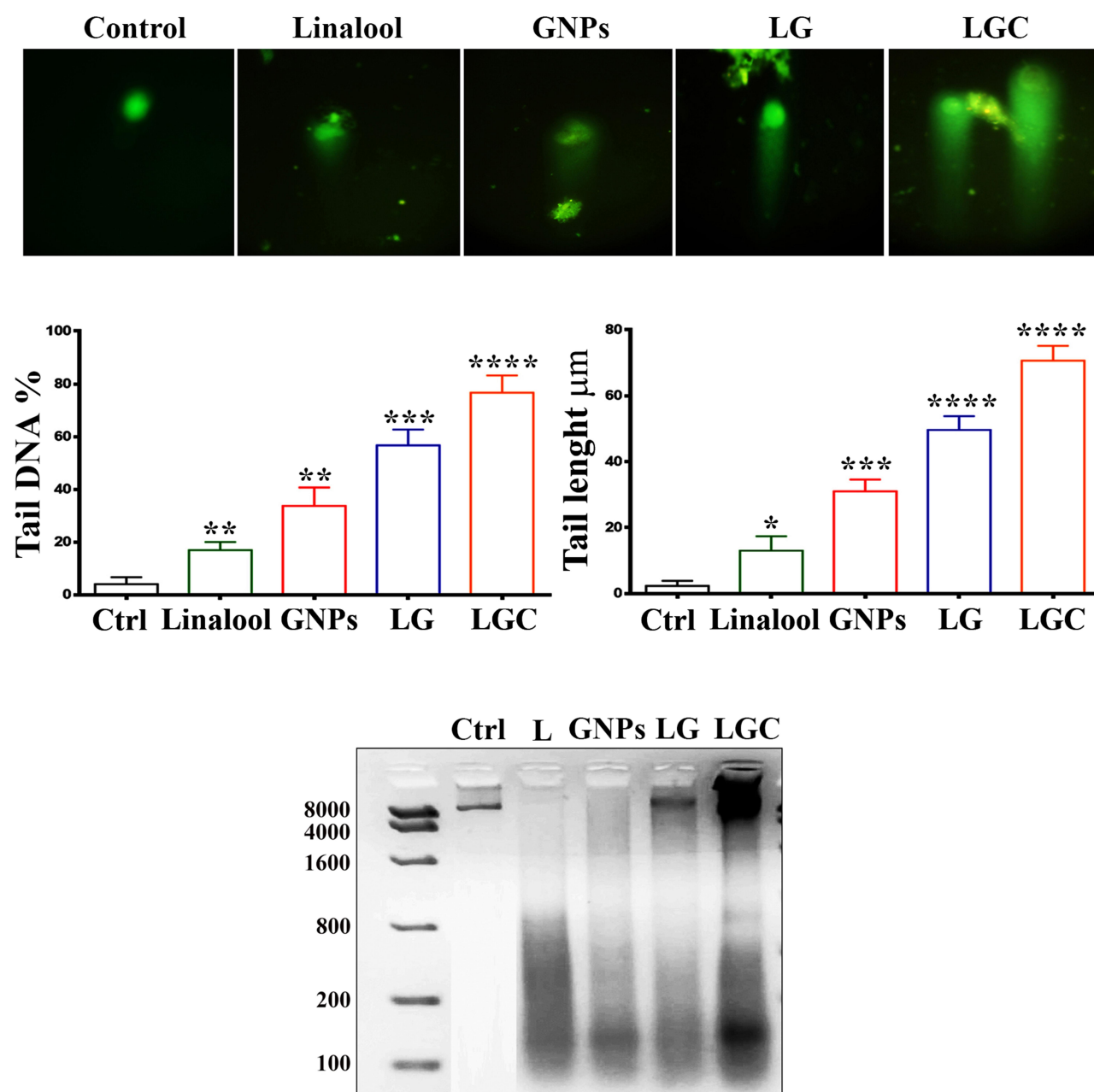
Figure 6 Genotoxicity of compounds in SKOV-3 cells. The upper panel show comet assay, which used to determine the different levels of DNA damage (long tail) in SKOV-3 cell line following treatment as indicated. Lower Panel showed DNA damage induced by tested compounds in SKOV-3 cell line was characterized by the percentage of DNA tail and tail length. The results are represented as the mean ± SD. Asterisks indicate statically different from control untreated cells, *$p \leq 0.05$, **$p \leq 0.01$, ***$p \leq 0.001$, ****$p \leq 0.0001$. DNA electrophoresis of SKOV-3 treated with tested compound as in indicated.
Abbreviations: GNP, gold nanoparticles; LG, linalool-gold nanoparticle; LGC, linalool-gold nanoparticle-CALNN.

implicated in the DNA repair system via the identification of DNA strand breaks and by acting as regulatory agents. In the current study, the results of the comet assay demonstrated a long tail length in cells treated with LG and LGC. These results indicate the induction of nucleic acid damage. Histone H2A phosphorylation can be used as a critical indicator of DNA damage, as it has the ability to form nuclear foci on the sites of damage and proceed as

a signal to induce other repair proteins. Cells with DNA damage exhibit increased migration of nucleic acid to the anode end.[47] The results also showed that untreated cells exhibited a halo localized around the cell nuclei. Moreover, the treated cells exhibited an increased length of nucleic acid migration. Thus, LG and LGC seem to have the ability to induce DNA fragmentation, indicating that these features constitute one of the characteristics of

apoptosis that can induce programmed cell death. The effects of the synthesized compounds on DNA were investigated as shown in Figure 6, represented by DNA fragmentation in SKOV-3 cells. The results revealed cellular apoptotic features such as a DNA ladder and smears. One of the biochemical properties involved in the apoptotic process is nuclear DNA crumbling, which indicates the crumbling and fragmentation of typical ladder DNA on agarose gel.[48,49] In contrast, the DNA gel electrophoresis method was used to determine the cell death caused by LG and LGC. Control cells did not exhibit any changes in fragmentation. Thus, the test compounds interacted with the DNA, leading to several structural or conformational changes that altered the metabolic function and caused damage to cellular components; this suggests that LG and LGC are capable of evoking fragmentation and damage in nucleic acid via different free radicals.[50] This specific DNA cleavage is caused by the activation of endogenous endonuclease, which is cleaved at the exposed linker region between nucleosomes.[51] The results of this study confirm the activities of LG and LGC, which induced cell death through the apoptotic pathway. The comet assay is one of the common experimental methods used for evaluating DNA damage, wherein cells with DNA damage exhibit increased migration of nucleic acids to the anode end.[47] Our results indicated that untreated cells exhibited a halo localized around the cell nuclei. Moreover, the treated cells exhibited an increase in the length of nucleic acid migration. LG and LGC had the ability to induce DNA fragmentation, indicating that these apoptotic features can induce programmed cell death. To examine the role of linalool, GNPs, LG, and LGC in the generation of ROS, SKOV-3 cells were tested for the production of ROS using fluorescence microscopy. ROS play an important role in the signaling of cells, apoptosis by stimulation, and the induction of mitochondrial-intrinsic events or lipid peroxidation, which lead to cell damage and death. The production of large amounts of ROS involves several nonreceptor-mediated stimuli, such as protein denaturation, oxidation of lipids, DNA damage, and expression of p53, which induce tumorigenesis or cell apoptosis. DHE is the best and most precise fluorescent stain that can be used for measuring ROS, such as superoxide. In the present study, the production of ROS was investigated by DHE staining, as shown in Figure 7. The results revealed that intracellular superoxide production was increased when SKOV-3 cells were treated with linalool, GNPs, LG, and LGC for 24 h compared with the control untreated cells. The outcome data revealed the high activity of LG and LGC to evoke the production of ROS. ROS are reactive molecules that are derived from the univalent reduction of oxygen, leading to the formation of different types of molecules (superoxide, hydroxyl radical, and hydrogen peroxide). These molecules act as secondary messengers that control different transduction signals. The production of a high level of superoxide will lead to a cytotoxic effect via the induction of oxidation of the base in the nucleic acid, which leads to cell death.[52]

Identification of the Localization of the Synthesized Compounds in the Treated Cells

The uptake of FITC-labeled LG and LGC into SKOV-3 cells was observed under a fluorescence microscope, and a single histogram peak was obtained, as shown in Figure 8 (upper panel). Nanoparticle uptake was found to be higher in drug-sensitive LG- and LGC-treated cells than in control cells. Moreover, the uptake of FITC-labeled LG and LGC was quantified by determining the median fluorescence intensity of the FITC signal using flow cytometry. The results suggested the internalization of FITC-labeled LG and LGC into SKOV-3 cells. The latter compound had the capacity to cause death and induce apoptosis because of its peptide size, biocompatibility, cell-penetrating ability, and the ability to bind to nuclear proteins. It was observed that the peptide can be taken up by specific cell organelles. The functionalization of GNPs with a cell-penetrating peptide was performed to improve the efficiency of live-cell uptake, wherein CALNN was basically trapped in the endoplasmic reticulum because of the excessive affinity of the ER for signal peptides and its capacity to penetrate the nucleus based completely on the nuclear pore complex.[53,54] The internalization process of the LG and LGC complexes was investigated using SEM. The SEM micrographs of SKOV-3 cells after treatment with LG and LGC complexes for 24 h revealed a change in the cell morphology from a spindle shape to an oval or round shape, with shrinkage and blebbing of the cell membrane and surface, as depicted in Figure 8 (lower panel). Our results indicated the internalization of the LG and LGC complexes, as observed by the adherence of these complexes onto the surface of treated SKOV-3 cells. The LG and LGC complexes were also found in the cytoplasm and around the nuclei. The results of SEM confirmed the
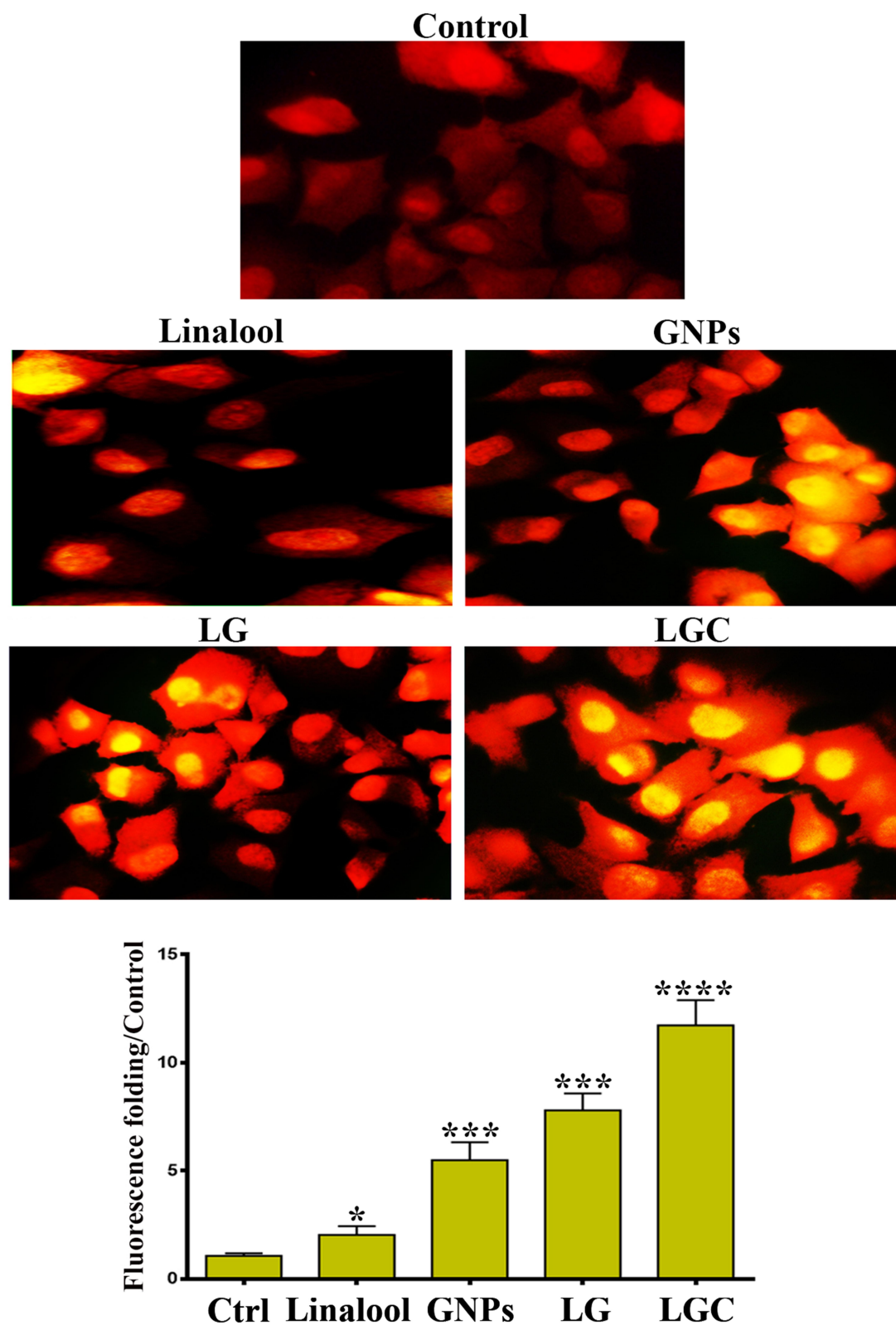
Control

Linalool

GNPs

LG

LGC

Figure 7 ROS Generation in SKOV-3 cells. Generation of ROS in SKOV-3 cells following treatment as indicated. Bar chart represents quantification of DHE fluorescence intensity at different treatment as indicated. The results are represented as the mean ± SD. Asterisks indicate statically different from control untreated cells, *p≤0.05, ***p≤0.001, ****p≤0.0001. DHE fluorescence folding increased when cells were treated with LG, and LGC. The yellow staining of nuclei refer to increased of the intracellular production of ROS. Scale bar 50µm.
Abbreviations: ROS, reactive oxygen species; DHE, dihydroethidium; GNP, gold nanoparticles; LG, linalool-gold nanoparticle; LGC, linalool-gold nanoparticle-CALNN; DHE, dihydroethidium.
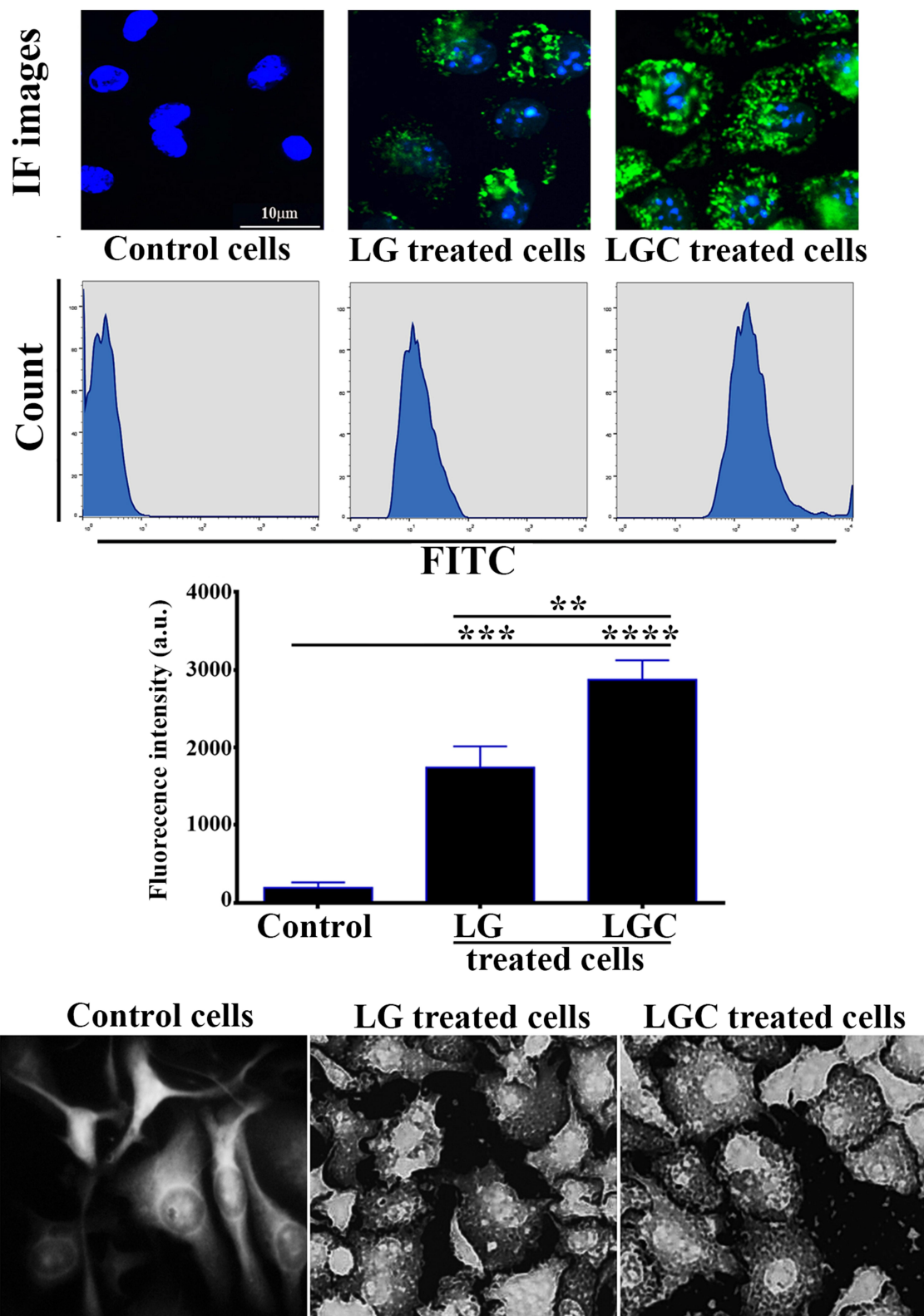
Figure 8 Detection and quantification of cellular uptake of FITC-labeled LG and LGC in SKOV-3 cells. Cellular uptake of FITC-labeled LG and LGC in SKOV-3 cells monitored by fluorescence microscopy after 12 h of incubation at 37 _C (scale bar: 10 μm). Flow cytometry histogram of cell count versus FITC intensity (FITC-A denotes FITC area) of FITC-labeled LG and LGC added to SKOV-3. Bar graphs represent the median fluorescent intensity of the FITC signal detected in SKOV-3 cells against the concentration of FITC-labeled LG and LGC. Data are representative of three sets of experiments. Data are represented as mean±SD. Asterisks indicate statically different from control untreated cells, **$p \leq 0.01$, ***$p \leq 0.001$, ****$p \leq 0.0001$. Lower panel represented SEM micrograph of SKOV-3 cells showed cellular uptake and internalization of LG, LGC complexes in cytoplasm and around of nuclei. Images showes blebs; cytoplasmic extrusions, membrane holes, and cellular change morphology and lysis.
Abbreviations: FITC, fluorescein isothiocyanate; LG, linalool-gold nanoparticle; LGC, linalool-gold nanoparticle-CALNN.

results of the cellular uptake of FITC-labeled LG and LGC complexes.

Mitochondrial Membrane Potential Assay

Matrix metalloproteinases (MMPs) are important biomarkers and potential therapeutic targets of tumors, in which mitochondrial dysfunction is a major characteristic of the cells that have undergone apoptosis. Qualitative and quantitative modification of mitochondria were identified via JC-1. In control cells, JC-1 shows the ability to assemble (J-aggregates); this compound also has the ability to exhibit a high and strong fluorescence signal (red), with excitement and emission at 560 and 595 nm, respectively.[55] Moreover, in apoptotic cells, JC-1 was found as a monomer with a lower fluorescence signal (red) in the 485 and 535 nm regions.[56] As shown in Figure 9A, mitochondria showed a highly red fluorescence signal in control cells, as a sign of mitochondrial activity, while cells treated with the synthesized compounds exhibited decreased red fluorescence with decreased mitochondrial activity. These results demonstrated that an increased amount of JC-1 accumulated in the treated groups. Thus, the integrity of mitochondria was lost by the induction of the depolarization of the mitochondrial membrane through LG and LGC. Mitochondria play a vital role in the stimulation of apoptotic events via different stimuli of cellular death. Alterations in this organelle are represented by the loss of its membrane potential ($\Delta\psi$m) and the release of the cytochrome c protein to the cytoplasm, resulting in the upregulation of caspase-3 through the caspase-9 pathway. In the present study, we detected apoptosis by flow cytometry assay according to the manufacturer's protocol. A decrease in the mitochondrial membrane potential is a significant and important indication of apoptotic cell death. The mitochondrial membrane potential was measured using the flow cytometric method after staining SKOV-3 cells with the Rh123 probe. We investigated the quantity of apoptotic SKOV-3 cells after treatment with the test compounds. A sizable increase in apoptosis upon treatment with these compounds was clearly observed, as shown in Figure 9B. SKOV-3 cells treated with linalool, GNPs, LG, and LGC for 24 h exhibited a great decrease in Rh123 staining, which indicated the reduction of the mitochondrial membrane potential compared with the control untreated SKOV-3 cells.

Apoptosis Proteomic Profile

After treating the SKOV-3 cells with the synthesized compounds for 24 h, we analyzed the major proteins responsible for cell death and apoptosis in this context using the Human Apoptosis protein array. As shown in Figure 10, we detected alterations in those proteins. Several proteins were upregulated or downregulated depending on their role in the apoptotic pathway. Moreover, many of these proteins, including BAX, Bad, Bim, cytochrome C, SMAC, and HtrA-2, play a major and significant role in the intrinsic apoptotic pathway. These proteins were considerably upregulated after treatment of the SKOV-3 cell line with LGC for 24 h. Other proteins that were upregulated included Bid, caspase-3, caspase-8, CD40, CD40 ligand, DR6, Fas, Fas ligand, Hsp60, HTRA, IGF-1, IGF-2, IGFBP1, IGFBP4, P21, P27, P53, survivin, TNFR-I, TNFR-II, TRAIL-1, TRAIL-2, TRAIL-3, and TRAIL-4 (Figure 10A). In contrast, the expression of the antiapoptotic proteins Bcl-2, Bcl-w, cIAP-2, XIAP, LIVIN, Hsp27, IGFBP5, IGFBP6, IGF-IR, TNF-A, TNF-B, and XIAP was inhibited (Figure 10B). Several studies have shown that Bcl-2 proteins, such as BAX, Bim, Bad, Bcl-2, and Bcl-w, play a major and important role in the mediation of the mitochondrial pathway by releasing cytochrome c from the mitochondria into the cytoplasm of cells, which triggers the formation of an apoptosome and leads to the activation of the downstream molecules of caspase-9, which play a major role in the induction of the activation of caspase-3 and caspase-7.[55] The results of the cellular protein expression investigation indicated that the apoptotic pathway is intrinsic. The markers SMAC/DIABLO and HtrA2/Omi have the ability to reduce the expression of proteins such as cIAP-2 and XIAP, as observed by the reduced expression levels of these proteins. Moreover, previous experiments demonstrated that the p53 tumor suppressor protein plays a major role in the induction of apoptotic death. In addition, p53 may be combined with the mitochondrial pathway by regulating the Bcl2 protein family, or may be implicated in cell-cycle arrest by inducing the expression of p21.[56] p53 also plays a role in the induction of p27, which is interlinked with the apoptotic stimulation as it is related to the apoptotic stimuli via an interconnection with the Bax protein.[57] In turn, our results also demonstrated the downregulation of HSP70 and HSP27 during apoptosis. In addition, proteins such as Bad, Bid, caspase-3, caspase-8, Fas, CD40, DR6, TNF, and TRAIL-4 were upregulated in SKOV-3 cells treated with LGC. These results demonstrated the association of SKOV-3 cells with the extrinsic pathway of apoptosis. An increase in caspase-8 expression can induce other caspases (caspase-3 and caspase-7) or has the ability to crosslink with the mitochondrial pathway by cleaving Bid to tBid. The results of the apoptosis proteome array
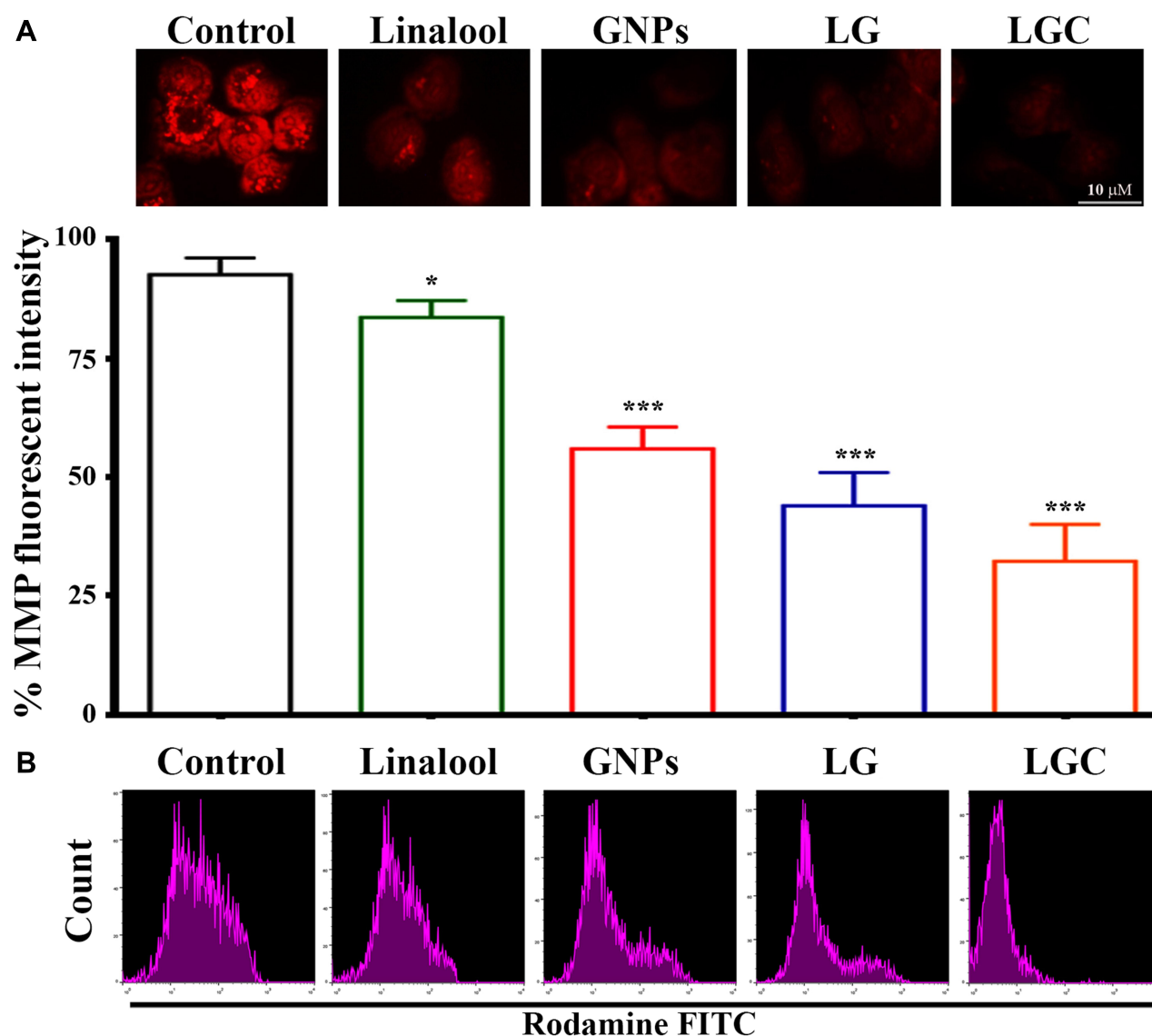
A

B

Figure 9 Dysfunction of MMP in SKOV-3 cells. The fluorescent intensity of MMP indicator JC 1 in control and treated cells as indicated. (**A**) Graph represented the statistical analysis of fluorescent intensity ratio. (**B**) Flow cytometry data in SKOV-3 cells were treated as indicated Rhodamine stain was used to investigate loss of Mitochondrial Membrane Potential. The data are represented as mean ± SD. Asterisks indicate statically different from control untreated cells, *p≤0.05, ***p≤0.001.
Abbreviations: LG, linalool-gold nanoparticle; LGC, linalool-gold nanoparticle-CALNN.

experiment performed in this study demonstrated that both the intrinsic pathway (through mitochondria) and the extrinsic pathway (through Fas, FTNFR, and TRAIL) have the ability to induce apoptosis in SKOV-3 cells treated with LGC.

Treatment with the Test Compounds Upregulated the Expression of Caspase-8 and p53

The previous assay clearly showed that LG and LGC have the ability to induce a mitochondrial-dependent apoptotic effect. Two major mechanisms are necessary for apoptosis

induction, ie, the extrinsic pathway (death receptor-mediated) and the intrinsic pathway (regulated at the level of mitochondria). The extrinsic pathway involves signals on the surface molecules (Fas/FasL) that lead to the recruitment of Fas-associated death domain (FADD).[58] The FADD–Fas complex has the ability to induce pro-caspase-8. This dynamic and important complex is referred to as the death-inducing signaling complex (DISC) and has the ability to activate and induce caspase-3, which leads to the induction of apoptosis.[59] The caspase-8 and p53 activities were investigated by flow cytometry and real-time PCR. The flow cytometry results
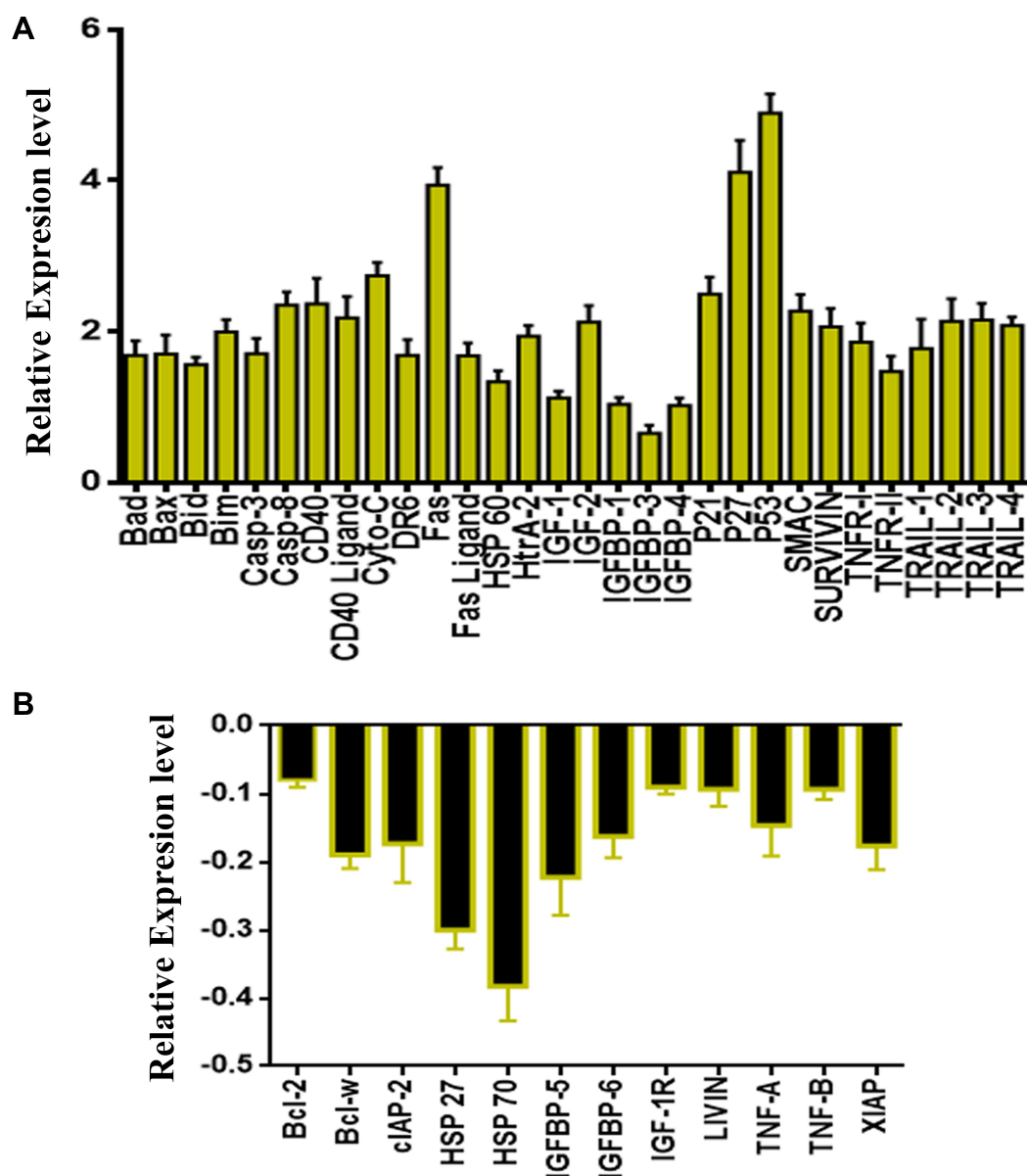
Figure 10 Quantitative analysis of the human apoptosis proteome profiler array in SKOV-3 cells. Cells were treated with LGC for 24 h, then cells were lysed and protein arrays were performed. Equal amounts (250 μg) of protein from each control and treated samples were used for the assay. (**A**) Representative bar graph of the apoptotic up-regulated proteins. (**B**) Bar graph shows the apoptotic down-regulated proteins. The results are represented as the mean ± SD.

shown in Figure 11A demonstrated that the cells treated with LG and LGC exhibited a marked shift toward the right for both caspase-8 and p53, which were designated as the apoptosome. Apoptosomes can be observed in apoptotic events, leading to the systematic disassembly of the cell. In the present study, we measured the levels of p53 and caspase-8 expression. The results showed that treatment of SKOV-3 cells with the test compounds led to a significant upregulation of both P53 and caspase-8 compared with the control (Figure 11B). Consequently, the

extrinsic and intrinsic apoptotic pathways led to the activation of caspase-3 in the apoptotic events. Caspase-3 imitates a major role in apoptosis and is specifically required for the fragmentation of nucleic acids, which leads to the characteristic apoptotic pattern of DNA ladder.[60]

Measurement of NF-κB Activity

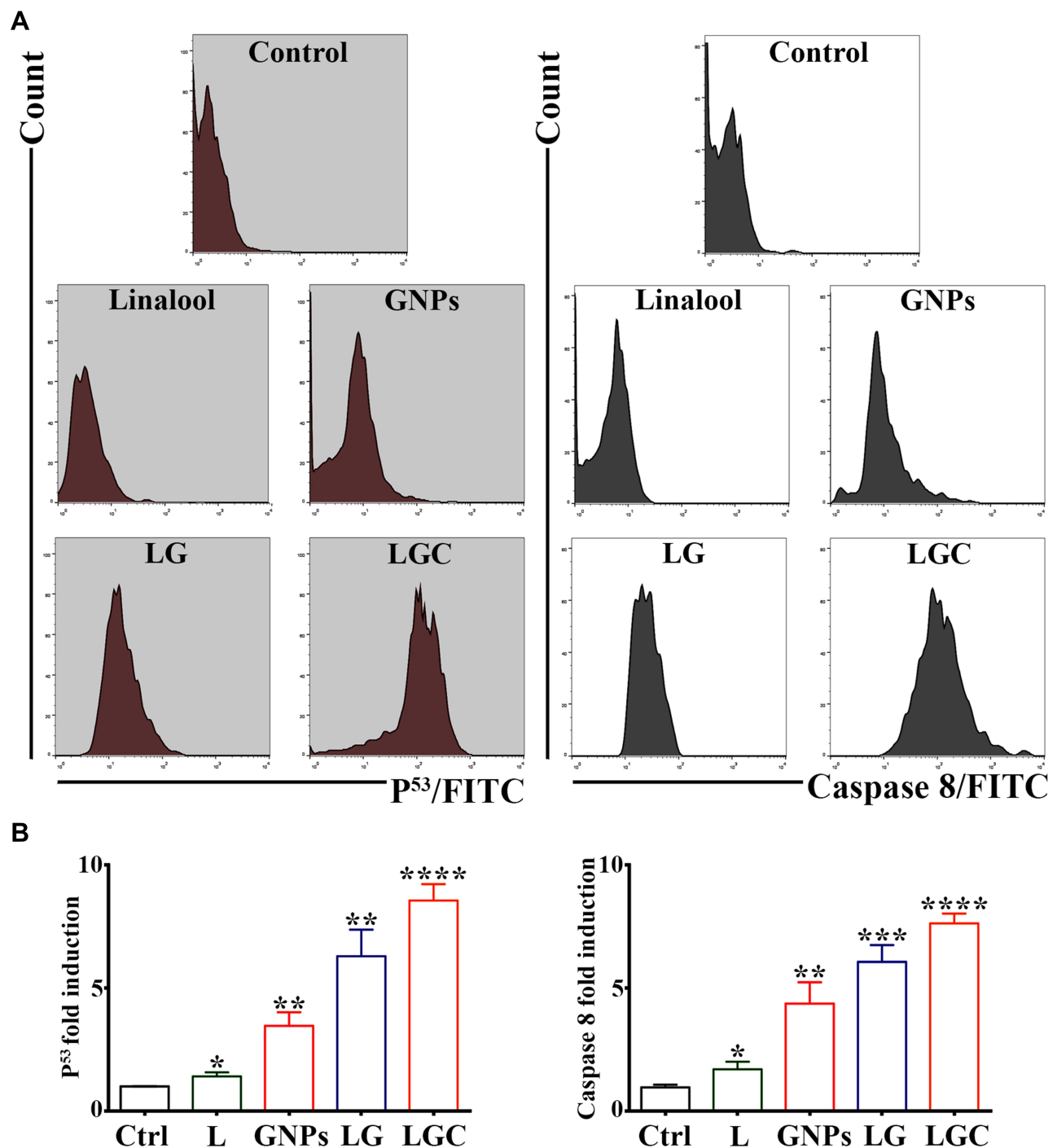NF-κB activity was evaluated in the cells that were treated with the synthesized compounds was evaluated. The

A

B

Figure 11 LG and LGC up regulated of caspase-8 and P[53] level in SKOV-3 cells. (**A**) SKOV-3 cells were treated as indicated. Fluorescence histograms of immunolabeled caspase-8 and P53 were assessed by flow cytometry. (**B**) Bar graph represented the expression of P53 and Caspase-8 levels in SKOV-3 cells after treated as indicated. Results are shown as mean ± SD. Asterisks indicate statically different from control untreated cells, *p≤0.05, **p≤0.01, ***p≤0.001, ****p≤0.0001.
Abbreviations: GNP, gold nanoparticle; LG, linalool-gold nanoparticle; LGC, linalool-gold nanoparticle-CALNN.

control cells without treatment exhibited increased intensity of the fluorescence signal of cytoplasmic NF-κB compared with that detected in cells treated with the synthesized compounds, which exhibited a low intensity of the fluorescence signals, as shown in Figure 12. SKOV-

3 cells that were exposed to LG and LGC were stimulated by TNF-α, which led to a considerable decrease in the intensity of cytoplasmic NF-κB. The results indicated the potential of LG and LGC to cause inhibition of the NF-κB signaling pathway in the SKOV-3 cell line. These findings
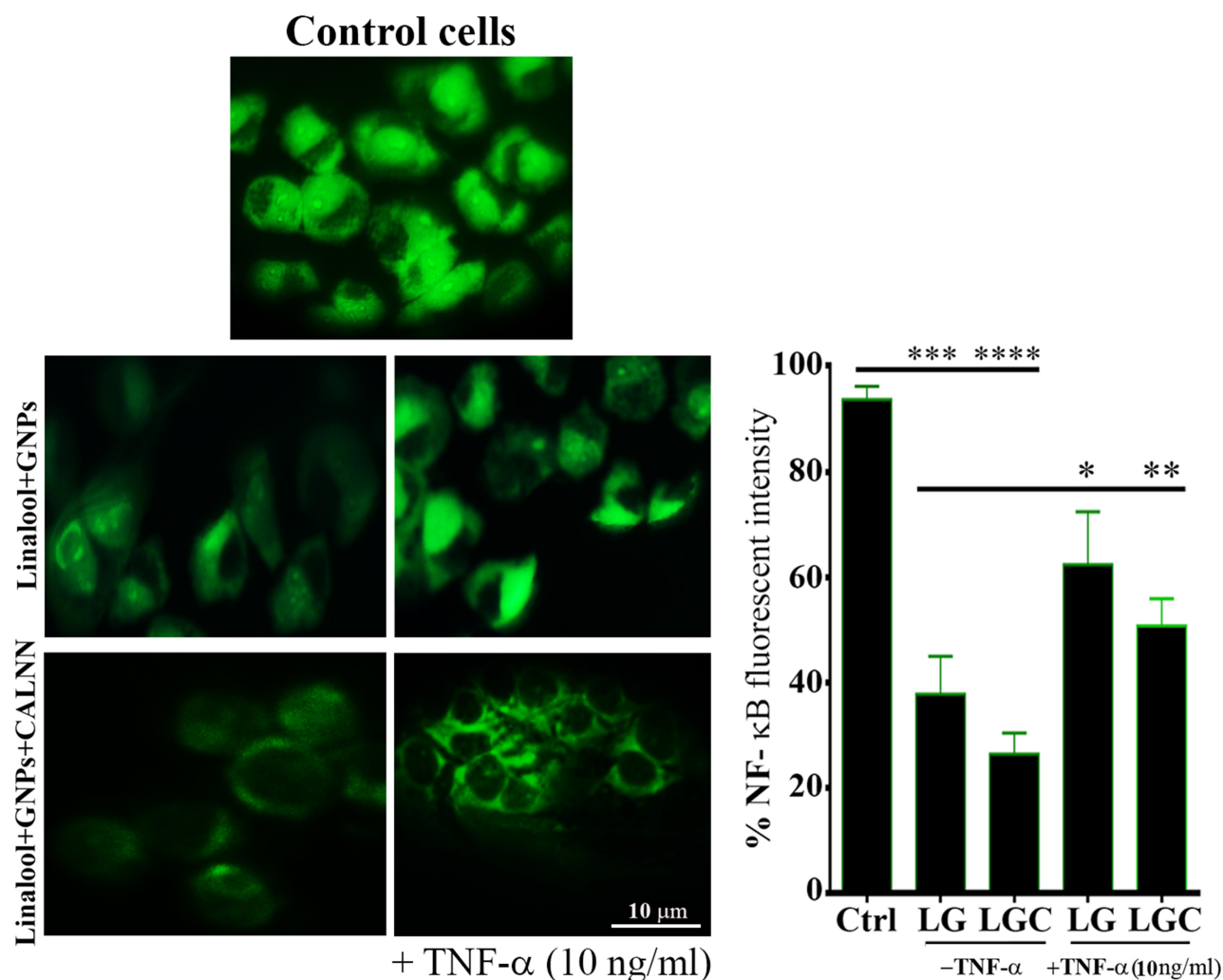
Figure 12 LG and LGC down-regulated of NF-κB activation in SKOV-3 cells. The fluorescence images showed NF-κB activation signaling in cells after treated as indicated in the presence and absence of TNF-α at concentration 10 ngmL-1. Chart represented quantitative analysis of three independent experiments. The results are represented as the mean ± SD. Asterisks indicate statically different from control untreated cells, ***p≤0.001, ****p≤0.0001, and statically different from treated cells as indicated in the presence and absence of TNF-α at concentration 10 ngmL-1, *p≤0.05, **p≤0.01.

Abbreviations: NF-κB, nuclear factor kappa-light-chain-enhancer of activated B cells; LG, linalool-gold nanoparticle; LGC, linalool-gold nanoparticle-CALNN; TNF-α, tumor necrosis factor-alpha.

suggest that NF-κB translocation could be blocked via LG and LGC, which are involved in apoptosis. The results also showed that both the extrinsic and intrinsic pathways may be involved in the stimulation of the apoptotic pathway by upregulating caspase-8 and p53 and blocking NF-κB translocation into the cytoplasm and nucleus. The consequences of the mitochondrial-intrinsic actions indicated by mRNA and the upregulation of p53, Bax, and cytochrome c could elicit mitochondrial damage and dysfunction by enhancing the levels of caspase-8.

Conclusion

A practical approach for the synthesis of a drug-delivery system by loading linalool onto GSH-modified GNPs conjugated with CALNN was developed in this study. The loading method represented an easier and more valid procedure, without the requirement of any additives for the synthesis of well-defined nanoparticles. The results showed that LG and LGC have high efficiency and should be given particular attention in anticancer drug-delivery systems. LG and LGC were extraordinarily more effective as antiproliferative agents against the SKOV-3 cell line than were linalool and GNPs alone. Furthermore, the results demonstrated that LG and LGC killed the ovarian cancer cells and induced apoptosis in the treated cells via the activation of caspase-8, p53, NF-κB, and Bax pathway. Moreover, both the extrinsic and intrinsic apoptotic pathways could stimulate apoptosis by upregulating caspase-8 and p53. In addition, they caused

the suppression of NF-κB translocation from the cytoplasm into the nucleus. The association between the events of mitochondrial-intrinsic pathways via mRNA and the upregulation of p53, Bax, and cytochrome c should elicit a loss of mitochondrial function, as evaluated based on the amount of caspase-8 activity. The results confirmed that these compounds may be used as a medicinal drug alone or in combination with other chemotherapeutics for treating different types of cancer cells.

Acknowledgments

Author Contributions

All authors made a significant contribution to the work reported, whether that is in the conception, study design, execution, acquisition of data, analysis and interpretation, or in all these areas; took part in drafting, revising or critically reviewing the article; gave final approval of the version to be published; have agreed on the journal to which the article has been submitted; and agree to be accountable for all aspects of the work.

Disclosure

All authors report no conflicts of interest in this work.

References

1. Shende P, Sardesai M, Gaud RS. Micro to nanoneedles: a trend of modernized transepidermal drug delivery system. *Artif Cells Nanomed Biotechnol*. 2018;46(1):19–25. doi:10.1080/21691401.2017.1304409
2. Daraee H, Eatemadi A, Abbasi E, Fekri Aval S, Kouhi M, Akbarzadeh A. Application of gold nanoparticles in biomedical and drug delivery. *Artif Cells Nanomed Biotechnol*. 2016;44(1):410–422. doi:10.3109/21691401.2014.955107
3. Medeiros Venancio A, Ferreira-da-Silva FW, da Silva-alves KS, et al. Essential oil of Ocimum basilicum L. and (-)-linalool blocks the excitability of rat sciatic nerve. *Evid Based Complement Alternat Med*. 2016;2016:9012605. doi:10.1155/2016/9012605
4. Guerrero YA, Bahmani B, Singh SP, Vullev VI, Kundra V, Anvari B. Virus-resembling nano-structures for near infrared fluorescence imaging of ovarian cancer HER2 receptors. *Nanotechnol*. 2015;26 (43):435102. doi:10.1088/0957-4484/26/43/435102
5. Anand P, Kunnumakkara AB, Sundaram C, et al. Cancer is a preventable disease that requires major lifestyle changes. *Pharm Res*. 2008;25(9):2097–2116. doi:10.1007/s11095-008-9661-9
6. Sugiura M, Ito S, Saito Y, et al. Molecular cloning and characterization of a linalool synthase from lemon myrtle. *Biosci Biotechnol Biochem*. 2011;75(7):1245–1248. doi:10.1271/bbb.100922

7. Chang M-Y, Shen Y-L. Linalool exhibits cytotoxic effects by activating antitumor immunity. *Molecules*. 2014;19(5):6694–6706. doi:10.3390/molecules19056694
8. Sun X-B, Wang S-M, Li T, Yang Y. Anticancer activity of linalool terpenoid: apoptosis induction and cell cycle arrest in prostate cancer cells. *Trop J Pharm Res*. 2015;14(4):619–625. doi:10.4314/tjpr.v14i4.9
9. Meireles DRP, Fernandes HMB, Rolim TL, et al. Toxicity and antitumor efficacy of Croton polyandrus oil against Ehrlich ascites carcinoma cells. *Rev Bras Farmacogn*. 2016;26(6):751–758. doi:10.1016/j.bjp.2016.05.014
10. Wang Y, Strohm EM, Sun Y, et al. Biodegradable polymeric nanoparticles containing gold nanoparticles and Paclitaxel for cancer imaging and drug delivery using photoacoustic methods. *Biomed Opt Express*. 2016;7(10):4125–4138.
11. Zhou G, Liu Y, Luo M, Xu Q, Ji X, He Z. Peptide-capped gold nanoparticle for colorimetric immunoassay of conjugated abscisic acid. *ACS Appl Mater Interfaces*. 2012;4(9):5010–5015. doi:10.1021/am301380q
12. Zhang X, Lin C, Lu A, et al. Liposomes equipped with cell penetrating peptide BR2 enhances chemotherapeutic effects of cantharidin against hepatocellular carcinoma. *Drug Deliv*. 2017;24(1):986–998. doi:10.1080/10717544.2017.1340361
13. Lee I-C, Ko J-W, Park S-H, et al. Comparative toxicity and biodistribution of copper nanoparticles and cupric ions in rats. *Int J Nanomedicine*. 2016;11:2883–2900.
14. Jabir MS, Taha AA, Sahib UI. Linalool loaded on glutathione-modified gold nanoparticles: a drug delivery system for a successful antimicrobial therapy. *Artif Cells Nanomed Biotechnol*. 2018;46(sup2):345–355. doi:10.1080/21691401.2018.1457535
15. Jabir MS, Taha AA, Sahib UI, Taqi ZJ, Al-Shammari AM, Salman AS. Novel of nano delivery system for Linalool loaded on gold nanoparticles conjugated with CALNN peptide for application in drug uptake and induction of cell death on breast cancer cell line. *Mater Sci Eng C*. 2019;94:949–964. doi:10.1016/j.msec.2018.10.014
16. Lin Z, Li Y, Xu T, et al. Inhibition of enterovirus 71 by selenium nanoparticles loaded with siRNA through bax signaling pathways. *ACS Omega*. 2020;5(21):12495–12500. doi:10.1021/acsomega.0c01382
17. Briñas RP, Hu M, Qian L, Lymar ES, Hainfeld JF. Gold nanoparticle size controlled by polymeric Au(I) thiolate precursor size. *J Am Chem Soc*. 2008;130(3):975–982. doi:10.1021/ja076333e
18. Lévy R, Thanh NTK, Doty RC, et al. Rational and combinatorial design of peptide capping ligands for gold nanoparticles. *J Am Chem Soc*. 2004;126(32):10076–10084. doi:10.1021/ja0487269
19. Sulaiman GM, Jabir MS, Hameed AH. Nanoscale modification of chrysin for improved of therapeutic efficiency and cytotoxicity. *Artif Cells Nanomed Biotechnol*. 2018;46(sup1):708–720. doi:10.1080/21691401.2018.1434661
20. Tailor CS, Goyal A. Antioxidant activity by DPPH radical scavenging method of ageratum conyzoides linn. leaves. *Am J Ethnomed*. 2014;1(4):244–249.
21. Seema D, Sandeep D, Sandeep K, Jaya Parkash Y, Novel A. Significant method for antioxidant activity utilizing microtitre-plate (resazurin reducing power assay). *Curr Opin Chem Biol*. 2012;6 (1):70–76.
22. Sulaiman GM, Waheeb HM, Jabir MS, Khazaal SH, Dewir YH, Naidoo Y. Hesperidin loaded on gold nanoparticles as a drug delivery system for a successful biocompatible, anti-cancer, anti-inflammatory and phagocytosis inducer model. *Sci Rep*. 2020;10(1):1–16. doi:10.1038/s41598-020-66419-6
23. Sulaiman GM. Molecular structure and anti-proliferative effect of galangin in HCT-116 cells: in vitro study. *Food Sci Biotechnol*. 2016;25:247–252. doi:10.1007/s10068-016-0036-4
24. Rieger AM, Nelson KL, Konowalchuk JD, Barreda DR. Modified annexin V/propidium iodide apoptosis assay for accurate assessment of cell death. *J Vis Exp*. 2011;(50):2597.

25. Sulaiman GM, Tawfeeq AT, Naji AS. Biosynthesis, characterization of magnetic iron oxide nanoparticles and evaluations of the cytotoxicity and DNA damage of human breast carcinoma cell lines. *Artif Cells Nanomed Biotechnol*. 2017;1–15.

26. Alsaedi IIJ, Taqi ZJ, Abdul Hussien AM, Sulaiman GM, Jabir MS. Graphene nanoparticles induces apoptosis in MCF-7 cells through mitochondrial damage and NF-KB pathway. *Mater Res Express*. 2019;6(9):095413. doi:10.1088/2053-1591/ab33af

27. Pal A. Photochemical synthesis of gold nanoparticles via controlled nucleation using a bioactive molecule. *Mater Lett*. 2004;58 (3):529–534. doi:10.1016/S0167-577X(03)00540-8

28. Shaw CF, Schaeffer NA, Elder RC, Eidsness MK, Trooster JM, Calis GHM. Bovine serum albumin-gold thiomalate complex: gold-197 Moessbauer, EXAFS and XANES, electrophoresis, sulfur-35 radiotracer, and fluorescent probe competition studies. *J Am Chem Soc*. 1984;106(12):3511–3521. doi:10.1021/ja00324a019

29. Chen J, Wang H, Long W, et al. Sex differences in the toxicity of polyethylene glycol-coated gold nanoparticles in mice. *Int J Nanomedicine*. 2013;8:2409–2419.

30. Gunaseelan S, Balupillai A, Govindasamy K, et al. The preventive effect of linalool on acute and chronic UVB-mediated skin carcinogenesis in Swiss albino mice. *Photoch Photobio Sci*. 2016;15 (7):851–860. doi:10.1039/C6PP00075D

31. Azam A, Ahmed AS, Oves M, Khan MS, Memic A. Size-dependent antimicrobial properties of CuO nanoparticles against Gram-positive and -negative bacterial strains. *Int J Nanomedicine*. 2012;7:3527–3535. doi:10.2147/IJN.S29020

32. Wen H, Jung H, Li X. Drug delivery approaches in addressing clinical pharmacology-related issues: opportunities and challenges. *AAPS J*. 2015;17(6):1327–1340. doi:10.1208/s12248-015-9814-9

33. Adjimani JP, Asare P. Antioxidant and free radical scavenging activity of iron chelators. *Toxicol Rep*. 2015;2:721–728. doi:10.1016/j.toxrep.2015.04.005

34. Alam MN, Bristi NJ, Rafiquzzaman M. Review on in vivo and in vitro methods evaluation of antioxidant activity. *Saudi Pharm J*. 2013;21(2):143–152. doi:10.1016/j.jsps.2012.05.002

35. Aazza S, Lyoussi B, Miguel MG. *Antioxidant and Antiacetylcholinesterase Activities of Some Commercial Essential Oils and Their Major Compounds: Molecules*. MDPI; 2011.

36. Zhang X-D, Wu H-Y, Wu D, et al. Toxicologic effects of gold nanoparticles in vivo by different administration routes. *Int J Nanomedicine*. 2010;5:771–781. doi:10.2147/IJN.S8428

37. Shabestarian H, Homayouni-Tabrizi M, Soltani M, et al. Green synthesis of gold nanoparticles using sumac aqueous extract and their antioxidant activity. *Mater Res*. 2017;20:264–270. doi:10.1590/1980-5373-mr-2015-0694

38. Czekanska EM. Assessment of cell proliferation with resazurin-based fluorescent dye. *Methods Mol Biol*. 2011;27–32.

39. El-Kassas HY, El-Sheekh MM. Cytotoxic activity of biosynthesized gold nanoparticles with an extract of the red seaweed Corallina officinalis on the MCF-7 human breast cancer cell line. *Asian Pac J Cancer Prev*. 2014;15(10):4311–4317. doi:10.7314/APJCP.2014.15.10.4311

40. Rahman MA, Ramli F, Karimian H, et al. Artonin E induces apoptosis via mitochondrial dysregulation in SKOV-3 ovarian cancer cells. *PLoS One*. 2016;11(3):e0151466. doi:10.1371/journal.pone.0151466

41. Li Y, Xu T, Lin Z, et al. Inhibition of enterovirus A71 by selenium nanoparticles interferes with JNK signaling pathways. *ACS Omega*. 2019;4(4):6720–6725. doi:10.1021/acsomega.8b03502

42. Copolovici DM, Langel K, Eriste E, Langel Ü. Cell-penetrating peptides: design, synthesis, and applications. *ACS Nano*. 2014;8 (3):1972–1994. doi:10.1021/nn4057269

43. Gupta R, Kashyap N, Rai B. Transdermal cellular membrane penetration of proteins with gold nanoparticles: a molecular dynamics study. *Phys Chem Chem*. 2017;19(11):7537–7545. doi:10.1039/C6CP08775B

44. Tang D, Kang R, Berghe TV, Vandenabeele P, Kroemer G. The molecular machinery of regulated cell death. *Cell Res*. 2019;29 (5):347–364.

45. Sever R, Brugge JS. Signal transduction in cancer. *Cold Spring Harb Perspect Med*. 2015;5(4):a006098. doi:10.1101/cshperspect.a006098

46. Khashan KS, Jabir MS, Abdulameer FA. Carbon nanoparticles decorated with cupric oxide nanoparticles prepared by laser ablation in liquid as an antibacterial therapeutic agent. *Mater Res Express*. 2018;5(3):035003. doi:10.1088/2053-1591/aab0ed

47. Lorenzo Y, Costa S, Collins AR, Azqueta A. The comet assay, DNA damage, DNA repair and cytotoxicity: hedgehogs are not always dead. *Mutagenesis*. 2013;28(4):427–432. doi:10.1093/mutage/get018

48. Li Y, Lin Z, Gong G, et al. Inhibition of H1N1 influenza virus-induced apoptosis by selenium nanoparticles functionalized with arbidol through ROS-mediated signaling pathways. *J Mater Chem B*. 2019;7(27):4252–4262. doi:10.1039/C9TB00531E

49. Samarghandian S, Shabestari MM. DNA fragmentation and apoptosis induced by safranal in human prostate cancer cell line. *Indian J Urol*. 2013;29(3):177–183. doi:10.4103/0970-1591.117278

50. Phaniendra A, Jestadi DB, Periyasamy L. Free radicals: properties, sources, targets, and their implication in various diseases. *Indian J Clin Biochem*. 2015;30(1):11–26.

51. Clark DJ. Nucleosome positioning, nucleosome spacing and the nucleosome code. *J Biomol Struct Dyn*. 2010;27(6):781–793. doi:10.1080/073911010010524945

52. Aggarwal V, Tuli HS, Varol A, et al. Role of reactive oxygen species in cancer progression: molecular mechanisms and recent advancements. *Biomolecules*. 2019;9(11):735. doi:10.3390/biom9110735

53. Kabachinski G, Schwartz TU. The nuclear pore complex – structure and function at a glance. *J Cell Sci*. 2015;128(3):423–429. doi:10.1242/jcs.083246

54. Wang C, Wang J, Liu D, Wang Z. Gold nanoparticle-based colorimetric sensor for studying the interactions of β-amyloid peptide with metallic ions. *Talanta*. 2010;80(5):1626–1631. doi:10.1016/j.talanta.2009.09.052

55. Sakamuru S, Attene-Ramos MS, Xia M. Mitochondrial membrane potential assay. *Methods Mol Biol*. 2016;1473:17–22.

56. Sivandzade F, Bhalerao A, Cucullo L. Analysis of the mitochondrial membrane potential using the cationic JC-1 dye as a sensitive fluorescent probe. *Bio Protoc*. 2019;9(1):e3128. doi:10.21769/BioProtoc.3128

57. Singh PK, Weber A, Häcker G. The established and the predicted roles of dynein light chain in the regulation of mitochondrial apoptosis. *Cell Cycle*. 2018;17(9):1037–1047. doi:10.1080/15384101.2018.1464851

58. Chen J. The cell-cycle arrest and apoptotic functions of p53 in tumor initiation and progression. *Cold Spring Harb Perspect Med*. 2016;6 (3):a026104. doi:10.1101/cshperspect.a026104

59. Lee D-H, Kim C, Zhang L, Lee YJ. Role of p53, PUMA, and Bax in wogonin-induced apoptosis in human cancer cells. *Biochem Pharmacol*. 2008;75(10):2020–2033. doi:10.1016/j.bcp.2008.02.023

60. Redza-Dutordoir M, Averill-Bates DA. Activation of apoptosis signalling pathways by reactive oxygen species. *Biochim Biophys Acta*. 2016;1863(12):2977–2992. doi:10.1016/j.bbamcr.2016.09.012